Abstract

Robust control theories and filtering techniques provide promising solutions for damping low-frequency inter-area oscillations. The objective of this research was to develop a systematic procedure of designing a distributed two-stage damping control system for power grid inter-area oscillations by applying separation and identification filter accompanied by robust control techniques. Practical considerations were emphasized in the proposed control design.

The first practical consideration was to select the control stabilizing signals and control site locations. Residual analysis were used to study the candidate signals and to evaluate their comparative strength. The most effective control signals were found to be line power flows and injected currents.

The second consideration was the robustness of the designed controller. System identification and separation were used to decouple the system in presence of faults and disturbances into three variations; fault and disturbance-free, fault-dependent and disturbance-dependent. This approach minimized the stringent trade-offs inherent in the control design objectives such as reference tracking, disturbance rejection and noise attenuation. As a result, the control design could be formulated into two main objectives. The first goal was related to reference tracking and oscillation damping which was achieved using the fault-free subsystem. The second aim referred to fault and disturbance suppression which was achieved through fault and disturbance-dependent subsystems. The control synthesis was formulated as mixed sensitivity H_∞ output-feedback problem with pole placement. Linear Matrix Inequality (LMI) approach was used to formulate the problem and to solve for a stabilizing controller.

The design procedure of two-stage robust control damping system was illustrated by two study systems. The first study was a single machine to infinite bus system. The second one was a two-area four-machine system.

The proposed architecture considerably minimized the overshoot when pole placement was not applied. For example, the overshoot was reduced by 41.98% in the first study case and by

17.60% in the second case study. If pole placement was required to achieve the minimum damping ratio, the improvement introduced by two-stage controller was less. For example, the overshoot was reduced by 0.4% only in the second case study. These results were drawn in comparison with the conventional centralized robust control. The proposed architecture successfully suppressed the impact of disturbances and faults on the operation of the system

This research was supported by the Government of Abu Dhabi to help fulfill the vision of the late President Sheikh Zayed Bin Sultan Al Nahyan for sustainable development and empowerment of the UAE and humankind.

"Ask and it will be given to you; seek and you will find; knock and the door will be opened to you."

– Matthew 7:7

Acknowledgments

I would like to express my deepest gratitude to my academic and research advisor Dr. Jimmy Peng for his guidance and constant support in helping me to conduct and complete this work. I would also like to express my gratitude to Dr. Haris Khalid for his assistance and useful feedback during my research. I highly appreciate their patience and unlimited time given to me during my work.

I want also to express my appreciation to the members of my committee Dr. Mohamed Elmoursi and Dr. Seddik Djouadi for all their supports and feedback.

I owe my sincere appreciation to my family who have been a constant support and engagement.I want to extend my profound appreciation to my great friends Jehad Kharraz, Dina Masri, Driss Lahjouji, Omar Saif and Mahmoud Shahin for the time we spent together during this wonderful journey.

Younes Isbeih,

Masdar City, May 24,2015.

Contents

List of Tables

List of Figures

1

INTRODUCTION

1.1 Motivations

Power system oscillations were observed in power systems as soon as synchronous generators were interconnected to provide more power capacity and more reliability [9]. These oscillations are the consequence of interactions among synchronous generators. Electromechanical oscillations are of the following types [4]:

- Intraplant mode oscillations
- Local plant mode oscillations
- Interarea mode oscillations
- Control mode oscillations
- Torsional modes between rotating modes

Intraplant mode is observed when generators swing against each other on the same power plant at frequencies of 2.0 to 3.0 Hz. The frequency of oscillation depends on the ratings of the generating units and the reactance connected to them [4]. For *local* mode, the synchronous machine oscillates against the rest of the system at a frequency of 1.0 to 2.0 Hz. *Inter-area* mode oscillations are observed over a large part of the network. It involves one or a group of generators swinging against one or a group of distant generators. The oscillation frequency

is approximately 0.3Hz. *Control* mode oscillations are associated with generators and poorly tuned exciters, governors, HVDC converters and SVC controls [4]. Finally, *Torsional* mode oscillations are caused by interactions related with turbine generator shaft in the frequency range of 10-46 Hz [4]..

Among different modes of oscillations, inter-area mode is the most difficult to damp in a stressed network. The presence of these modes restrains the amount of power flow on the transmission lines between the regions which contains groups of coherent generators [10]. They can become more poorly damped as the transmission capacity of tie-lines is increased. In modern grids, inter-area oscillations are often induced by disturbances. For example, 0.6 Hz in the Hydro-Quebec system[11], 0.2 Hz in the western North-American interconnection [12], 0.15 to 0.25 Hz in Brazil [13], and 0.19 to 0.36 Hz in the UCTE/CENTREL interconnection in Europe [14]. Some of major system failures due to oscillations are [15]:

- Detroit Edison (DE-Ontario-Hydro (OH)-Hydro Quebec (HQ(1960s,1983).
- Finland-Sweden-Norway-Denmark (1960s).
- Saskatchewan-Manitoba Hydro-Western Ontario (1966).
- Western Electric Coordinating Council (WECC)(1964,1996).
- South East Australia (1975).
- Scotland-England (1978)
- Western Australia (1982,1983).
- Ghana-Ivory Coast (1985).

Therefor, this research is motivated by the objectives of designing and implementing damping control with system identification and separation and thus enhancing the damping low-frequency inter-area modes. This is a relevant issue to Abu Dhabi due to the recent establishment of GCC interconnection. A. Al-Ebraihm et. al,[16], examined the presence of poorly damped inter-area oscillations in GCC system. They found that the interaction of North and south parts will change the shape of the existing oscillation modes and new inter-area modes will be experienced. Accordingly, this research proposes an improved robust control architecture to increase the damping of low-frequency inter-area oscillations which could occur in GCC interconnection in the future.

1.2 Literature Review on Robust Damping Control for Power Systems

New generating units are being added to the electric utility in US since the late 1950s [2]. Those units were equipped with continuously-acting voltage regulators. It was noticed that the voltage regulator action had a crucial effect on the dynamic stability of a power system as these units represented a larger percentage of the generating capacity. Small magnitude low- frequency oscillations are observed to present often for long periods of time. The presence of such oscillations limited, in some cases, the amount of power transfer over transmission lines. For example, a natural frequency of load swing at about 0.1 Hz was recorded on the 230-kV transmission line, which linked the interconnected power systems of the Northwest and that in the Southwest of US [17],[18].

Two modes of low-frequency oscillations are observed in large inter-connected power systems; local and inter-area oscillation modes. Local mode (1-2.0 Hz) is related with rotor angle modes of a single machine or plant against the other parts of the power system; inter-area mode (0.1 - 1 Hz) is involved with subgroups of machines oscillating against each other in different areas [2]. In 1965, C. Concordia [19] studied the dynamical performance of interconnected power system following disturbance. He found that for two large systems connected via weak tie line, the amortisseur damping becomes very small in contrary to small power systems where amortisseur damping represents the most important source of damping. M. Klein et. al [20] studied the nature of inter-area oscillations in power systems. They investigated the effects of the system structure, generator modeling, and the excitation type in addition to system loads.

It was found in [21],[22] that damping torques could be produced by applying special supplementary signals derived from tie-line power or frequency differences. This led to the development of power system stabilizers (PSS) to provide additional damping to these modes by modulating the excitation system. E.V. Larsen and D.A.Swann presented the main concepts related with implementing Power System Stabilizers using ac bus frequency electrical power inputs and shaft speed in a three-part paper [23],[24], [25]. The stabilizer must add electrical torque component on the machine rotor. The damping is provided when the produced component is in-phase with speed deviations. The added PSSs to the excitation systems are found to be the most economically feasible damping controls [9].

In recent years, different types of controls have been introduced to power systems. For exam-

ple, Flexible AC Transmission (FACTS) devices such as Thyristor controlled series capacitor (TCSC) and Static VAr compensator (SVC) were found to be both practical and economic [26], [27], [28], [29], [30], [31]. This comes in accordance with the rapid advances in power electronics area. Super-conducting magnetic energy storage (SMES) devices were also applied for damping control design [15].

Meanwhile, different control approaches were applied in the damping controller design. In the literature, damping controller were designed using some conventional control methods. These include the classical pole placement method [2], damping torque analysis [29], linear quadratic Gaussian (LQG), [32] and adaptive control [33]. A nominal operating point is used by almost all of these methods. This point is selected from a set of different operating conditions. However, power systems are highly nonlinear and the model uncertainty which results from the mismatches between the actual model of a power system and the one used in control design make it difficult to achieve a good controller design using only one single nominal operating point [34].

The power system stability is not guaranteed by controllers designed for the optimal performance at the chosen operating conditions. The development of modern robust control techniques offers a solution to the aforementioned shortcomings of conventional methods. The main purpose of robust control design is to obtain closed-loop systems that are stable and meet a priori specified performance objectives despite the presence of nonlinearities and plant uncertainty [34]. In literature two main technique were applied in robust control design; the H_∞ technique and the structured singular value (SSV or μ). These approaches were adopted for inter-area oscillations damping using PSSs, SMES, and FACTS. M.Kelin et al., [20], presented an H_∞ control design for a Thyristor controlled series compensator to improve inter-area oscillations damping in power systems. The solution for the standard H_∞ optimization problem was found by solving two Riccati equations. The analytical approach for standard H_∞ is based on finding a positive semi definite solution to Riccati equation [8]. The solution requires no iterations. However, the design controller based on Riccati equation approach suffers from pole-zero cancellations between the plant and the controller [35]. In addition, G.N. Taranto et al. [30] presented a systematic robust decentralized design based on solving Riccati equation for tuning multiple FACTS devices. SVC and TCSC were implemented in a 3-area,6-machine system in order synthesize a robust controller for damping interarea modes .

1.3 Objectives and Contributions

The objectives of this thesis is to propose a systematic procedure of designing a two-stage damping control system for low-frequency inter-area oscillations in power systems. Several practical issues are considered in this thesis like measurements and control sites selection as well as controller robustness evaluation. The main contributions of this thesis are:

1. Proposed a systematic procedure to design a centralized two-stage damping control systems and demonstrated its effectiveness to damp inter-area oscillations. The controller receives remote measurements, which has good observability with regards to the modes to be damped. Control actions are provided through FACTS devices,namely Static Var Compensator (SVC).

2. Demonstrated that controllabilty/observability based residual analysis could be effective in studying the candidate signals and evaluating their comparative strength.

3. Accurately estimated and separated disturbances and faults using unknown input observer (UIO). Three variations are obtained; fault and disturbance-free, fault-dependent and disturbance-dependent. The proposed architecture could achieve a good improvement in the damping of the inter-area modes in addition to suppressing the impact of faults and disturbances on power system operation.

4. Demonstrated that mixed-sensitivity H_∞ output-feedback control could be applied to the two-stage damping controller design with better results in comparison with those obtained by only applying control design to the system with faults and disturbances.

1.4 Thesis Organization

This thesis is organized into five chapters. Chapter 1 provides a detailed literature review of the state-of-art about damping of inter-area oscillations in power systems. It discusses the implementation of PSS, FACTS and SMES in power systems. In addition, the application of robust control synthesis for system oscillations damping are summarized.

Chapter 2 is a detailed analysis of mathematical models adopted to describe the dynamic performance of power system. These include the dynamic modeling of synchronous generators, exciter systems, power system stabilizers (PSS), governor systems in addition to electrical loads.

Modeling of static VAr compensators are also illustrated. The obtained model is called Differential Algebraic Equations (DAE). It consists of the nonlinear equations of the power system components and the algebraic equations which describe the voltage and injected current at each bus in the network. The DAE model will be linearized about a steady operating point. The development of a linearized model allows us to utilize the analysis techniques offered by Modal analysis. The linearized model will be used later for system identification and robust control design. This chapter presents also the study case used in the thesis; the Two-area, 4 machines system.

Chapter 3 describes a systematic procedure for two-stage robust control synthesis for damping low-frequency inter-area oscillations. Residual analysis are used to study the candidate measurements and to evaluate the controllers performance at different control sites. An unknown input observer (UIO) design is formulated for states and outputs coordinate transformation and faults and disturbance estimation. Three subsystems are obtained after applying system identification after which robust control design is applied. The robust control design is formulated as a mixed-sensitivity H_∞ output-feed problem with pole placement and is resolved in the LMI framework.

Chapter 4 will present two studied examples. The first one is the single machine to infinite bus system. The second study system is the two-area four-machine system.

Chapter 5 summarizes the findings of this research and lists several topics for the future work.

2

MODELING

2.1 Introduction

Electric power is produced by a group of synchronous generators at a power plant and transmitted to end-users through a complex network consisting of transformers, transmission lines and switching devices. A reliable operation is ensured by the ability of a power system to withstand the different types of disturbances. Accordingly, power system stability problem is largely related to maintaining synchronous operation. The dynamic performance of a power grid is affected by different types of devices with a variety of response rates and characteristics. This results in a highly nonlinear system. Every major element within the power network could affect the overall system stability. This chapter discusses the characteristics and modeling of main elements used in power grids.They are essential for understanding and modeling stability of power systems.

2.2 Power System Modeling

2.2.1 Synchronous Generator

In modern power systems, synchronous generators produce the main bulk of electric energy. An understanding of their characteristics and modeling of their dynamic performance is important to the study of power system stability [36]. The dynamic equations of a sixth-order synchronous

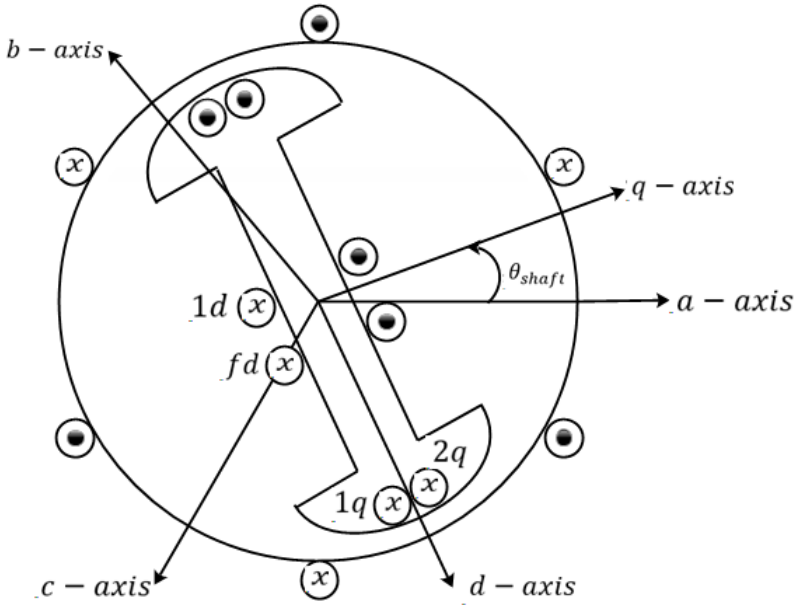

Figure 2.1: Synchronous generator schematic diagram [1]

generator i, which is shown in Fig 2.1 model can be stated as:

$$\dot{\delta}_i = \omega_i - \omega_s \tag{2.1}$$

$$\begin{aligned}\dot{\omega}_i = {} & \frac{\omega_s}{2H}[T_{mi} - D(\omega_i - \omega_s) - \frac{(X''_{di} - X_{lsi})}{(X'_{di} - X_{lsi})}E'_{qi}I_{qi} - \frac{(X'_{di} - X''_{di})}{(X'_{di} - X_{lsi})}\psi_{1di}I_{qi} \\ & - \frac{(X''_{qi} - X_{lsi})}{(X'_{qi} - X_{lsi})}E'_{di}I_{di} + \frac{(X'_{qi} - X''_{qi})}{(X'_{qi} - X_{lsi})}\psi_{2qi}I_{di} + (X''_{qi} - X''_{di})I_{qi}I_{di}]\end{aligned} \tag{2.2}$$

$$\begin{aligned}\dot{E'_{qi}} = {} & \frac{1}{T'_{doi}}[-E'_{qi} - (X_{di} - X'_{di})\{-I_{di} - \frac{(X'_{di} - X''_{di})}{(X'_{di} - X_{lsi})^2} \\ & (\psi_{1di} - (X'_{di} - X_{lsi})I_{di} - E'_{qi})\} + E_{fdi}]\end{aligned} \tag{2.3}$$

$$\begin{aligned}\dot{E'_{di}} = {} & -\frac{1}{T'_{qoi}}[E'_{di} + (X_{qi} - X'_{qi})\{I_{qi} - \frac{(X'_{qi} - X''_{qi})}{(X'_{qi} - X_{lsi})^2}(-\psi_{2qi} \\ & + (X'_{qi} - X_{lsi})I_{qi} - E'_{di})\}\end{aligned} \tag{2.4}$$

$$\dot{\psi}_{1di} = \frac{1}{T''_{doi}}[-\psi_{1di} + E'_{qi} + (X'_{di} - X_{lsi})I_{di}] \tag{2.5}$$

$$\dot{\psi}_{2qi} = -\frac{1}{T''_{qo}}[\psi_{2qi} + E'_{di} - (X'_{qi} - Xlsi)I_{qi}] \tag{2.6}$$

for $i = 1, 2, \ldots, m$,where,

m	:	total number of generators
δ_i	:	generator rotor angle
ω_i	:	rotor angular speed
E'_{qi}	:	transient emf due to field flux linkage
E'_{di}	:	transient emf due to flux-linkage in q-axis damper coil
ψ_{1di}	:	sub-transient emf due to flux-linkage in d-axis damper
ψ_{2qi}	:	sub-transient emf due to flux-linkage in q-axis damper
I_{di}	:	d-axis component of stator current
I_{qi}	:	q-axis component of stator current
$X_{di}, X'_{di}, X''_{di}$	:	synchronous, transient and sub-transient reactances, respectively along d-axis
$X_{qi}, X'_{qi}, X''_{qi}$	:	synchronous, transient and sub-transient reactances, respectively along q-axis
T'_{do}, T''_{do}	:	d-axis open-circuit transient and sub-transient time constants
T'_{qo}, T''_{do}	:	q-axis open-circuit transient and sub-transient time constants

In this thesis, the synchronous generator is represented by a sub-transient model with four equivalent coils on the rotor as described in [1]. In addition, the rotor dynamics are assumed to be much slower in comparison with the stator transients. As a result, the terminal bus quantities are used to relate the stator quantities through set of algebric equations rather than the differential state equations. The following states the stator algebraic equations:

$$V_i \cos(\delta_i - \theta_i) - \frac{(X''_{di} - X_{lsi})}{(X'_{di} - X_{lsi})} E'_{qi} - \frac{(X'_{di} - X''_{di})}{(X'_{di} - X_{lsi})} \psi_{1di} + R_{si} I_{qi} - X''_{di} I_{di} = 0 \tag{2.7}$$

$$V_i \sin(\delta_i - \theta_i) + \frac{(X''_{qi} - X_{lsi})}{(X'_{qi} - X_{lsi})} E'_{di} - \frac{(X'_{qi} - X''_{qi})}{(X'_{qi} - X_{lsi}))} \psi_{2qi} - R_{si} I_{di} - X''_{qi} I_{di} = 0 \tag{2.8}$$

for $i = 1, 2, \ldots, m$, where,

V_i	:	the voltage at generator terminal
R_{si}	:	the armature resistance
X_{lsi}	:	armature leakage reactance

2.2.2 Exciter

The generators are assumed to be equipped with slow excitation system (IEEE-DC1A). The block diagram of IEEE-DC1A is shown in Fig. 2.2

The block diagram represents field controlled DC commutator exciters with continuously

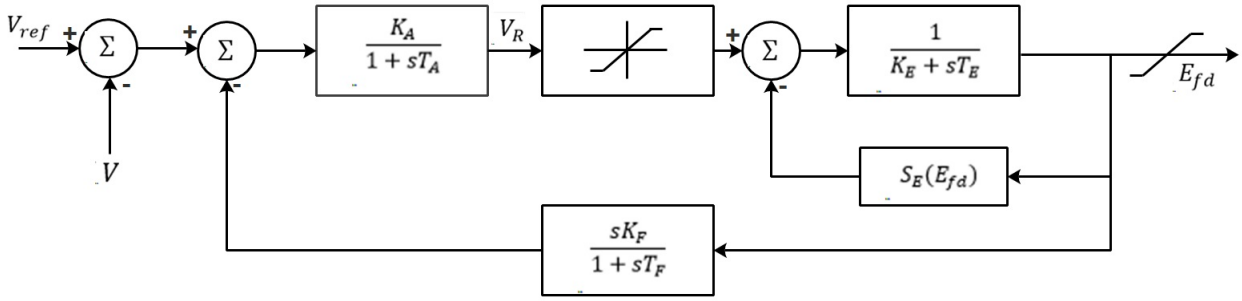

Figure 2.2: IEEE type DC1A excitation system model [2]

acting voltage regulators. This configuration may be separately excited or self-excited. K_E is selected so that $V_R = 0$ for self-excited operation. This represents operator action of tracking the voltage regulator by periodically trimming the shunt field rheostat setpoint. A separately excited exciter can be obtained by setting $K_E = 1$. The term $S_{ex}(E_{fd})$ accounts for the nonlinear exciter saturation curve, where it is typically given by:

$$S_{ex}(E_{fd}) = A_{ex}e^{B_{ex}E_{fd}}. \tag{2.9}$$

The dynamic behavior of an IEEE-DC1A type may be described as follows:

$$\dot{E}_{fdi} = -\frac{1}{T_{Ei}}[K_{Ei}E_{fdi} + E_{fdi}A_{ex}e^{B_{ex}E_{fdi}} - V_{ri}] \tag{2.10}$$

$$\dot{V}_{ri} = \frac{1}{T_{Ai}}[\frac{K_{Ai}K_{Fi}}{T_{Fi}}R_{Fi} + K_{Ai}(V_{refi} - V_{tri}) - \frac{K_{Ai}K_{Fi}}{T_{Fi}}E_{fdi} - V_{ri}] \tag{2.11}$$

$$\dot{R}_{Fi} = \frac{1}{T_{Fi}}[-R_{Fi} + E_{fdi}] \tag{2.12}$$

where,

V_{tri} : a state variable represents the measured voltage after the sensor lag block

V_{ri} : the scaled output of the amplifier which is applied to the field of the separately excited main exciter.

E_{fdi} : field voltage

R_{Fi} : rate feedback

2.2.3 Power System Stabilizer (PSS)

Auxiliary stabilizing signal(s) can be used by power system stabilizer (PSS) to control generator's excitation. This will provide additional damping to the rotor oscillations of the generator. A component of electrical torque must be produced by the stabilizer in phase with the rotor

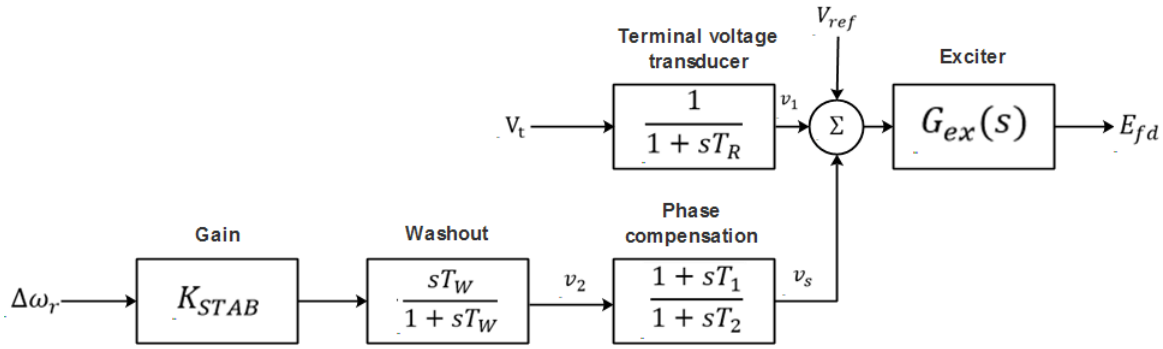

Figure 2.3: Power system stabilizer model [2]

speed deviations. As a result, speed deviation signal is used by PSS to control generator excitation. Fig. 2.3 shows the basic block diagram of one phase compensation PSS. The PSS in Fig. 2.3 is represented by three blocks: a phase compensation, a washout and a gain. The amount of damping provided by the PSS is determined by the stabilizer gain K_{STAB}. Practical considerations limit the amount of damping that can be added by the PSS. The signal washout block works as a high-pass filter, with time constant T_W sufficiently high to permit signals related with oscillations in ω_r to pass unchanged. The washout block prevents modifying the terminal voltage due steady changes in speed. The appropriate phase-lead characteristic is provided by the phase compensation block. It compensates for the phase lag between the machine electrical (air-gap) torque and the excitation system input . Based on the above described PSS model, the mathematical model can be developed as follows:

$$\dot{v}_{2i} = K_{STAB}\dot{\omega}_i - \frac{1}{T_W}v_{2i} \tag{2.13}$$

$$\dot{v}_{si} = \frac{T_1}{T_2}\dot{v}_{2i} + \frac{1}{T_2}v_{2i} - \frac{1}{T_2}v_{si} \tag{2.14}$$

2.2.4 Governor

The shaft speed along with the number of magnetic poles of the machine determines the frequency of the ac voltage at the terminals of machine's armature winding. The shaft of the synchronous generator's rotor is coupled and driven by prime mover's shaft. As a result, the steady-state speed of a synchronous machine is determined by the speed of the prime mover. In this thesis, steam turbines are assumed to drive the rotor's shaft. In steam power plants, steam is supplied to the chest by a steam boiler. The steam chest contains pressurized steam that enters a high pressure (HP) turbine through a steam valve. The steam valve position determines the me-

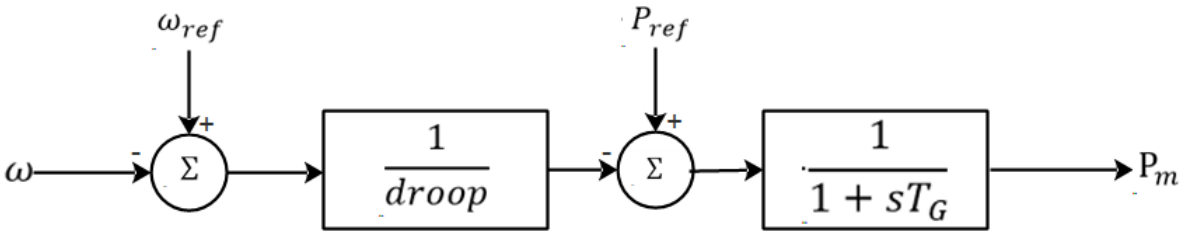

Figure 2.4: Governor model block diagram [3]

chanical torque of a synchronous machine. The governor is used to control the valve position by comparing the sensed frequency or speed of the generator and the desired value. The governor model is shown in Fig. 2.4, it's dynamic behavior can be represented as follows:

$$T_{SVi}\dot{P}_{SVi} = -P_{SVi} + P_{Ci} - \frac{1}{R_{Di}}(\frac{\omega_i}{\omega_s} - 1) \tag{2.15}$$

$$R_{Di} = \frac{2\pi droop_i}{\omega_s} \tag{2.16}$$

where

P_{SVi} : Valve power

P_{Ci} : Reference power

$droop_i$: speed droop expressed in $Hz/per-unitmegawatts$

R_{Di} : speed regulation

2.2.5 Static VAr Compensators (SVC)

The SVC is installed in the transmission network to maintain voltage by reducing the impact of system disturbances on the voltages at load bus terminals. SVC has fast dynamic response, so it is often installed when voltage collapse or transient instability cannot be prevented by the slow mechanically switched capacitors. Fig. 2.5 shows the block diagram of the SVC used in this thesis. The differential equations which represent the dynamic behavior of a SVC are expressed as:

$$\dot{B}_{svc} = \frac{1}{T_{svc}}[-B_{svc} + (1 - \frac{T_{v1}}{T_{v2}})V_{r-svc} - \frac{K_v T_{v1}}{T_{v2}}V_{t-svc}] + \frac{K_v T_{v1}}{T_{v2}T_{svc}}[V_{ss-svc} + V_{ref}] \tag{2.17}$$

$$\dot{V}_{r-svc} = \frac{1}{T_{v2}}[-V_{r-svc} - K_v V_{t-svc} + K_v V_{ref} + K_v V_{ss-svc}] \tag{2.18}$$

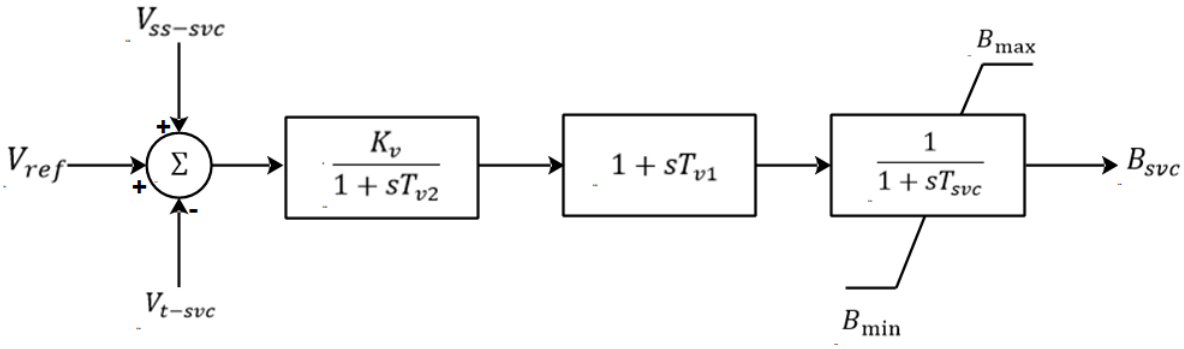

Figure 2.5: Static VAr Compensator (SVC) block diagram [4]

V_{t-svc}	:	the SVC terminal voltage
V_{ref}	:	the voltage reference
V_{ss-svc}	:	supplementary signal for damping inter-area modes
K_v	:	the gain of the controller
T_{svc}	:	the SVC thyristor control action time constant
T_{v1} and T_{v2}	:	time constants used to adjust the frequency gain
B_{svc}	:	the effective susceptance of the SVC
B_{max} and B_{min}	:	specify the range of compensation

2.2.6 Load

Voltage-dependent functions can be used to incorporate load dynamics into power system model. The load at any bus i is given by

$$P_{Li} = P_{Lio}\left(\frac{V_i}{V_{io}}\right)^{n_{pi}} \quad i = 1,\ldots,n \tag{2.19}$$

$$Q_{Li} = Q_{Lio}\left(\frac{V_i}{V_{io}}\right)^{n_{qi}} \quad i = 1,\ldots,n \tag{2.20}$$

where P_{Lio} and Q_{Lio} represent the nominal real and reactive powers at bus i with the associated voltage magnitude V_{io}, and n_{pi}, n_{qi} represent load indices. As a result, three types of load may be obtained:

1. Constant power load ($n_p = n_q = 0$)
2. Constant current load ($n_p = n_q = 1$)
3. Constant impedance load ($n_p = n_q = 2$)

2.2.7 Network Power Flow Equations

The following set of equations describe the network power flow equations for the generator buses:

$$V_i \cos(\delta_i - \theta_i) I_{qi} - V_i sin(\delta_i - \theta_i) I_{di} - \sum_{k=1}^{k=n} V_i V_k [G_{ik} \cos(\theta_i - \theta_k) + B_{ik} sin(\theta_i - \theta_k)] = 0 \quad (2.21)$$

$$-V_i \sin(\delta_i - \theta_i) I_{qi} - V_i cos(\delta_i - \theta_i) I_{di} - \sum_{k=1}^{k=n} V_i V_k [G_{ik} \sin(\theta_i - \theta_k) - B_{ik} \cos(\theta_i - \theta_k)] = 0 \quad (2.22)$$

for $i = 1, 2, \ldots, m$. The following gives, for the non-generator buses, the Power balance equations:

$$P_{Li}(V_i) + \sum_{k=1}^{k=n} V_i V_k [G_{ik} \cos(\theta_i - \theta_k) + B_{ik} \sin(\theta_i - \theta_k)] = 0 \quad (2.23)$$

$$Q_{Li}(V_i) + \sum_{k=1}^{k=n} V_i V_k [G_{ik} \sin(\theta_i - \theta_k) - B_{ik} \cos(\theta_i - \theta_k)] = 0 \quad (2.24)$$

for $i = m+1, \ldots, n$,where n is the total number of buses in the system.

2.3 Linearization of Power System Model

In the previous section, dynamic models were summarized for synchronous machine along with the associated regulating devices. The resultant synchronous generator can be characterized by a thirteenth-order model. The dynamic states vector for this model are:

$$x_d = [\delta \quad \omega \quad E'_d \quad E'_q \quad \psi_{1d} \quad \psi_{1q} \quad E_{fd} \quad V_r \quad R_F \quad v_2 \quad v_s \quad P_{SV}] \quad (2.25)$$

Equations (2.1) - (2.24) describe the complete dynamic performance of an interconnected power grid. This model can be rewritten as follows:

$$\dot{x} = f(x, y, u) \quad (2.26)$$

$$0 = g(x, y) \quad (2.27)$$

Equations (2.26) - (2.27) form the Dynamic Algebraic Equations (DAE) model of the power system dynamics. The state vector x contains the dynamic states of synchronous generator,

whereas the vector y contains both the I_{d-q} and $\bar{V}$. I_{d-q} is the direct and quadrature component of injected current into bus i, V is its phasor voltage. The vector u includes the control inputs. Equation (2.27) describes the network and the stator algebraic equations in the power-balance form. The vector y can be partitioned into load-flow equations and the other algebraic equations as:

$$y = [I^t_{d-q}\theta_1 V_1 \dots V_m | \theta_2 \dots \theta_n V_{m+1} \dots V_n]^t \tag{2.28}$$

$$= [y^t_a | y^t_b]^t \tag{2.29}$$

where y_b corresponds to the load-flows variables, and the vector y_a corresponds to the other algebraic variables. The number of machines and buses in the power system are denoted by m and n, respectively. The dynamic behavior of power systems, around an equilibrium point, according to the small signal theory, can be analyzed with a model linearized around this point. The obtained linear model is valid only in the neighborhood of the equilibrium point. It's only valid for analyzing the dynamics of the system under small disturbances. Linearizing (2.26) and (2.27) around an operating point gives:

$$\Delta\dot{x} = A_1\Delta x + B_1\Delta I_g + B_2\Delta V_g + E_1\Delta U \tag{2.30}$$

$$0 = C_1\Delta x + D_1\Delta I_g + D_2\Delta V_g \tag{2.31}$$

$$0 = C_2\Delta x + D_3\Delta I_g + D_4\Delta V_g + D_5\Delta V_l \tag{2.32}$$

$$0 = D_6\Delta V_g + D_7\Delta V_l \tag{2.33}$$

where $\Delta I_g = \begin{bmatrix} \Delta I_d \\ \Delta I_q \end{bmatrix}$, $\Delta V_g = \begin{bmatrix} \Delta\theta_g \\ \Delta V_g \end{bmatrix}$, $\Delta V_l = \begin{bmatrix} \Delta\theta_l \\ \Delta V_l \end{bmatrix}$, $\Delta U = \begin{bmatrix} \Delta T_M \\ \Delta V_{ref} \end{bmatrix}$, ΔV_g and ΔV_l are the generator and load bus voltages, respectively.

Equations (2.30) - (2.33) represents the linearized model for a multimachine system that has m machines and n buses. These equations result from linearizing the machine dynamic equations in addition to stator and network algebraic equations. Please refer to [1] for complete derivation of the linear model. Equations (2.30) - (2.33) could be described by the general form of linearized state space model of power systems after eliminating ΔI_g from (2.30) - (2.32) using (2.31). The operator Δ is omitted as all linear equations use variables that denote deviations

from the equilibrium point.

$$\dot{x} = Ax + Bu \tag{2.34}$$

$$y = Cx + Du \tag{2.35}$$

Here x is the power system state variables vector, y is the measured output variables vector. A is power system state matrix, B is the control input matrix, C is output matrix and D is feedforward matrix.

The equations (2.34)-(2.35) represent a combination of ordinary differential equations (ODE). This system is predominantly used for state space control design techniques. The state space representation can be transformed to frequency domain using Laplace transform as follows:

$$G(s) = \frac{Y(s)}{U(s)} = C(sI - A)^{-1}B + D \tag{2.36}$$

where s is the Laplace operator or complex frequency. The steady state response of the power system model to a sinusoidal input is referred to as the frequency response. The output of the system differs from the applied input in amplitude and phase only. This is valid only for linear systems. The power system transfer function $G(s)$ can be used in determining zeros and poles of the plant. Input signals with frequency at the zero of the system will be blocked and will not affect the output.

2.4 Modal Analysis and Small Signal Stability Evaluations

Having the dynamic model of a power system written in the general state space representation enables us to apply modal analysis. In addition, small signal stability of the power system can be studied. The eigenvalues of the matrix A are given by the values of the scalar parameter λ for which there exist non-trivial solutions (i.e, other than $\phi = 0$) to the equation:

$$A\phi = \lambda\phi \tag{2.37}$$

where

A : An $n \times n$ power system matrix

ϕ : An $n\times$ 1 vector

The eigenvalues λ can be determined after rearranging (2.37) as:

$$\det(A - \lambda I) = 0 \tag{2.38}$$

The n solutions of (2.38) are the eigenvalues of A and have the form of $\sigma \pm j\omega$. The eigenvalues are used to study the stability of the system.

1. *A real eigenvalue* corresponds to a non-oscillatory mode. A positive real eigenvalue represents aperiodic instability, whereas the negative real eigenvalue corresponds to a decaying mode. A faster decay is obtained when the the magnitude of the real part is larger.

2. *Complex eigenvalues* occur in conjugate pairs, where each pair corresponds to an oscillatory mode. The real part (σ) gives the damping ratio and the imaginary part (ω) gives the actual or damped frequency of oscillation. Damped oscillations are obtained for negative real eigenvalue, whereas an oscillation of growing amplitude is obtained by positive real part.

Accordingly, for complex eigenvalues:

$$\lambda = \sigma \pm j\omega \tag{2.39}$$

The actual or damped frequency in Hz is determined by:

$$f = \frac{\omega}{2\pi} \tag{2.40}$$

The damping ratio may be obtained by:

$$\zeta = \frac{-\sigma}{\sqrt{\sigma^2 + \omega^2}} \tag{2.41}$$

The decay rate of oscillation's amplitude is determined by the damping ratio ζ. The amplitude decays to 37% of the initial value in $\frac{1}{|\sigma|}$ seconds or in $\frac{1}{2\pi\zeta}$ cycles of oscillation. For any eigenvalue λ_i, the $n-$column vector ϕ_i which satisfies (2.37) is called the *right eigenvector* of system matrix A associated with the eigenvalue λ_i. Similarly, the *left eigenvector* related with the eigenvalue λ_i is the n-row vector ψ_i which satisfies:

$$\psi_i A = \lambda_i \psi_i \qquad i = 1, 2, \ldots, n \tag{2.42}$$

Assuming that [2]:

$$\Phi = \begin{bmatrix} \phi_1 \phi_2 \dots \phi_n \end{bmatrix}$$
$$\Psi = \begin{bmatrix} \psi_1^T \psi_1^T \dots \psi_n^T \end{bmatrix}^T$$

Λ is a diagonal matrix which contains the diagonal elements $\lambda_1, \lambda_2, \dots, \lambda_n$.

where Φ,Ψ and Λ are $n \times n$ matrices. The diagonal matrix Λ can be obtained as follows:

$$\Phi^{-1} A \Phi = \Lambda \tag{2.43}$$

$$\Psi A \Psi^{-1} = \Lambda \tag{2.44}$$

The right and left eigenvectors are normalized for convenience as:

$$\Psi \Phi = I \tag{2.45}$$

The ODE power system model can be transformed using the modal matrix Φ into modal coordinates z through a transformation $x = \Phi z$:

$$\dot{z} = \Lambda z + \Psi B u \tag{2.46}$$

$$y = C \Phi z + D u \tag{2.47}$$

The dynamics of the transformed system are governed by set of uncoupled first order differential equations. Each i-th mode in the right eigenvector may be used to examine the response of a particular state variable x_i. The *right eigenvector* gives the mode shape, i.e., the relative activity of the state variables when a particular mode is excited. The *left eigenvector* establishes the combination of state variables which represents only the i-th mode. The association between the state variables and the modes are measured by the *participation matrix* (P) [2].

$$P = [P_1 \quad P_2 \dots P_n] \tag{2.48}$$

with

$$P_i = \begin{bmatrix} P_{1i} \\ P_{2i} \\ \vdots \\ P_{ni} \end{bmatrix} = \begin{bmatrix} \phi_{1i} \psi_{i1} \\ \phi_{2i} \psi_{i2} \\ \vdots \\ \phi_{ni} \psi_{in} \end{bmatrix} \tag{2.49}$$

The $P_{ki} = \phi_{ki}\psi_{ik}$ is referred to as the *participation factor*. The element on the k-th row and i-th column of the modal matrix Φ is represented by ϕ_{ki}. In addition, the element on the i-th row and k-th column of Ψ is represented by ψ_{ik}. Assuming that $\Psi = \Phi^{-1}$, the decoupled ODE system (2.46)-(2.47) can be rewritten as:

$$\dot{z} = \Lambda z + B'u \tag{2.50}$$

$$y = C'z + Du \tag{2.51}$$

where

$$B' = \Phi^{-1}B \tag{2.52}$$

$$C' = C\Phi \tag{2.53}$$

It can be interpreted from (2.50) that if the i-th row of matrix B' is zero, the inputs have no effect on the i-th mode and the i-th mode is said accordingly to *uncontrollable*. In addition, the mode i-th is said to be *unobservable* if the i-th column of the matrix C' is zero. In this case, the variable z_i will not contribute to the formation of the outputs. The $n \times r$ matrix B' is termed as the *mode controllability matrix*, and the $m \times n$ matrix as the *mode observability matrix*. The D matrix in the power system described by (2.34) - (2.35) is usually a zero matrix. Thus, $G(s)$ may be rewritten as follows:

$$G(s) = \frac{Y(s)}{U(s)} = C(sI - A)^{-1}B \tag{2.54}$$

$$= C\Phi[sI - \Lambda]^{-1}\Psi B \tag{2.55}$$

Since Λ is a diagonal matrix, we may write

$$G(s) = \sum_{k=1}^{n} \frac{R_k}{s - \lambda_k} \tag{2.56}$$

where

$$R_i = C\phi_i\psi_k B \tag{2.57}$$

R_i is referred to as modal residue being the product of modal observability $(C\phi_i)$ and modal controllability $(\psi_i B)$. The residue R_k of a particular mode k gives the measure of that mode's

sensitivity to a feedback between the output and the input. The residue is a complex variable so its magnitude and phase are important. Less control efforts (gain) are required for high magnitudes. As a result, the best location for installing PSS or FACTS in a power system can be identified using residual analysis. If there is no pole zero cancellation, the poles of the power system transfer function $G(s)$ are given by the eigenvalues of A according to (2.56). The solution of the following equations gives the zeros of power system transfer function $G(s)$:

$$\sum_{k=1}^{n} \frac{R_i}{s-\lambda_i} = 0 \tag{2.58}$$

2.5 Model Reduction Operation

Modern control design techniques, such as H_∞ and Linear Quadratic Gaussian (LQG), produce controllers which have at least similar order equals to that of the power system model. They usually have higher order because of the inclusion of weighting functions. Therefore, it is necessary to simplify the power system model in order to avoid controller complexity with regards to practical implementation and to ease the design procedure. However, the reduced power system model must be a good approximation of the original system in order to be used for control design. The central idea in *model order reduction problem* is that for a given power system model $G(s)$ with high-order n, find a low-order approximation $G_r(s)$ with order r such that the infinity norm of the error transfer function $\|G(j\omega) - G_r(j\omega)\|_\infty$ is sufficiently small [4]. $\|\Delta\|_\infty$ is the **H**-Infinity (**L**2 gain) of a stable power system Δ. This norm denotes the peak value of the magnitude of the power system transfer function over the whole frequency range. In the literature, no good solution was obtained for the **H**-Infinity optimal model reduction [37]. Another system norm is adopted which is the Hankel norm $\|\Delta|_H$. The hankel norm relates past inputs to future system outputs while ignoring any power system response before time 0. Accordingly, the hankel norm of a stable system is never larger than its **Hi**Infinity norm. As opposed to the **H**-Infinity optimal model reduction, the hankel optimal model reduction has a solution in the literature. As a result,*optimal Hankel norm approximation* is adopted in this thesis to reduce the order of power system model [**?**].

For the power system state space representation $G(s) \stackrel{s}{=} (A,B,C,D)$. The solutions P and Q

of the following equations:

$$PA^T + AP + BB^T = 0 \tag{2.59}$$

$$QA + A^T Q + C^T C = 0 \tag{2.60}$$

are called the controllability and observability grammian,respectively. $\sigma(PQ) = diag(\sigma_1, \sigma_2, \ldots, \sigma_n)$ is the singular value of the product of controllability and observability grammian. The *sigma* are Hankel singular values (HSV) of $G(s)$ where $\sigma_i = \sqrt{\lambda_i(PQ)}$. The Hankel singular values are ordered as $\sigma_1 \geq \sigma_2 \geq \sigma_3 \ldots \sigma_n$. The Hankel norm is defined as the largest singular value σ_1, that is, $\|G\|_\infty = \sigma_1$. In Optimal Hankel norm approximation approach, an optimization problem [37] is solved to obtain the order r of the reduced model. The optimization problem is formulated such that for a given power system model $G(s)$ of order n, a reduced order model is to be found of degree k such that the Hankel norm of the error $\|G(s) - G_k(s)\|_H$ is minimized. The largest HSV of the error transfer function is to be minimized by the solution for the optimization problem.

3

TWO STAGE ROBUST CONTROL DESIGN

3.1 General Design Procedure

The design of two-stage robust control for inter-area modes damping includes the following steps:

1. Development of the complete nonlinear model of the studied system: Matlab, [7], is utilized to obtain the multi-machine model of the power system under study. A subtransient model with four coils on the rotor is used to model all generators with governor, exciter and conventional PSS.

2. Model linearization and small signal analysis: A linear model is obtained by linearizing the full-order nonlinear model about a chosen operating point. The developed linear model is then used to conduct small signal analysis. Modal analysis is used to determine the frequencies, damping ratios and mode shapes for local and inter-area modes.

3. Selection of measurements and control sites: Stabilizing signals are selected based on the easiness of obtaining the measurements which should have a high observability with respect to a particular inter-area mode. Residual analysis [38] are used to study the candidate signals and to evaluate their comparative strength. Residual analysis are used to examine the controllers performance at different sites with respect to an inter-area mode.

4. Linear model reduction: The designed controller has an order which is equals the open-loop system order including the weighting functions. Some power system models may contain hundreds of states. Accordingly, it is mandatory to reduce the order of the power system model to ease the control design procedure and to avoid practical complexity in the synthesized controller. However, the reduced power system model should maintain the main characteristics of the original system [39]. In this research, the optimal hankel norm approximation is adopted for the model reduction task. The robust control toolbox in Matlab is utilized [40].

5. First stage - system identification: An unknown input observer (UIO) is used to separate the disturbances and faults from the model. This is done by decoupling the state and output the state and output equations into three variations; fault and disturbance-free, fault-dependent and disturbance-dependent. Accordingly, three variations will be obtained at the first stage;system output,fault and disturbance. The main findings of [41] are adopted in UIO design.

6. Second stage - robust control design: A controller is synthesized using the LMI approach to the multi-objective H_∞ control for each variation obtained at the first stage. Regional pole placement may be required to achieve the minimum damping ratio. Acceptable transient response, robust stability and robust performance should be met by the designed controller.

7. Closed-loop verification: Matlab is used to evaluate the controller performance in the closed-loop system. The controlled output from each variation is then sent to the distributed fusion center to feed the original system back.

3.2 Two Stage Control System Architecture

There are two approaches to design damping controllers, the centralized and decentralized. The first one employs a set of remote control signals with different modal contents [26]. These signals are often called as ”global signals” to show that they posses information with respect to the dynamics of the whole network as opposed to local stabilizing signals which are used in decentralized approach. The later one lacks sufficient observability for some of the important inter-area modes [42]. A local signal (e.g., generator terminal voltage or generator rotor speed)

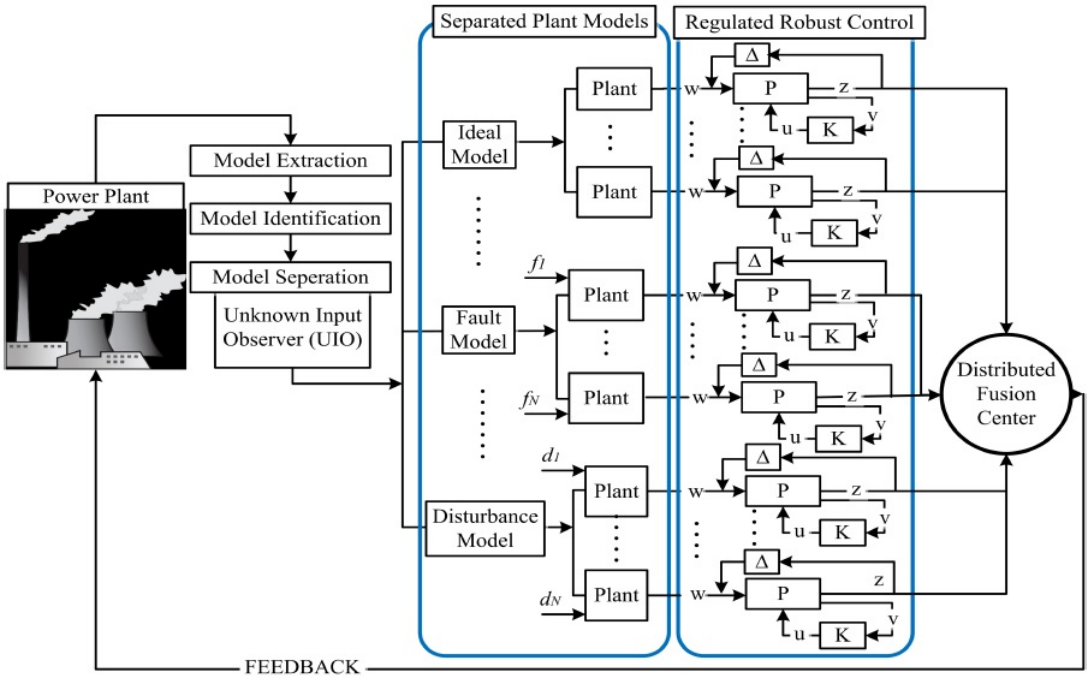

Figure 3.1: Two-stage robust control damping system

has the largest residue for local modes. However, the local signal may not be the one with maximum observability for inter-area modes. Maximum observability with respect to a given mode could be associated with a signal that is obtained from a remote location or as a combination of signals from different locations. Synchronous phasors and stabilizing control signals can be delivered at a high sampling rate (e.g., at a 30-Hz) [43] due to the recent development in wide-area measurement (WAM) technologies using phasor measurements (PMUs). The application of the centralized controllers utilizing global signals,from an economic viewpoint, may be more economically feasible in comparison with adding new control equipment [44].

The installation of PSSs in a power plant results in a well damped local oscillation modes. However, the control signals used by those PSSs are local ones and often have insufficient observability with respect to a particular inter-area modes [45]. As a result, poorly damped inter-area modes are observed. Accordingly, a wide-area controller may be used to provide supplementary control signals to the PSS from wide-area measurements. Improvement in inter-area modes damping is obtained.

Fig.3.1 shows the proposed centralized two-stage robust control architecture. In the first stage, an (UIO) is used to obtain three decoupled variations from the state and output equations. These variations are:

1. Fault and disturbance-free

2. Fault-dependent

3. Disturbance-dependent

Once the separated models for variation of system output, fault and disturbance have been developed from N number of sensors, a multi-objective H_∞ output feedback control is designed for each model variation using LMI approach. This represents the second stage of the proposed architecture. The centralized controller in the control center collects all measurements calculates the control signals and sends them to control locations.

3.3 Selection of Measurements and Control Locations

The selection of stabilizing control signals in addition to control sites location are an important consideration in the design of damping control systems. For FACTS devices, generator angular speed, line active power and line current are examples for the widely adopted input signals. Reference [10] concluded that the measured transmission line-current represents the most suitably auxillary input stabilizing signal for SVC for enhancing the damping. Similar findings were also found by G. Rogers [9]. References [46], [47] select locally measured active power as input signals and references [48], [31] select generator angular speed as input signals. [2] used terminal frequency, shaft speed and integral of power as input signals for PSS. The MIMO state-space model of the studied power system may be given as:

$$\dot{x} = Ax + Bu \tag{3.1}$$

$$y = Cx \tag{3.2}$$

where x is the $n \times 1$ state vector, u is the $m \times 1$ input vector and y is the $p \times 1$ measured output vector; A, B and C are state,input and output matrices which have the dimensions $(n \times n), (n \times m)$ and $(p \times n)$, respectively. Assuming that matrix A has n distinct eigenvalues $(\lambda_k, k = 1, \ldots, n)$ and the associated matrices of right and left eigenvectors are ϕ and ψ, respectively. The sensitivity of the kth eigenvalue to a feedback between the output and the input is given by the residue R_k. Residues can be used to measure the participation of mode k in the dynamics between inputs and outputs. Residue matrix R_k associated with kth natural mode is a $p \times m$

matrix and defined as the product of the mode's observability and controllability:

$$R_k = C\phi_k\psi_k B \tag{3.3}$$

The residue-based attributes of controllability $m_{ci}(k)$ and observability $m_{oj}(k)$ related with mode k may be formulated in a normalized form as[38]:

$$m_{ci}(k) = \frac{\|R_k(:,i)\|}{\|R_k\|}, \quad (i = 1,\ldots,m) \tag{3.4}$$

$$m_{oj}(k) = \frac{\|R_k(j,:)\|}{\|R_k\|}, \quad (j = 1,\ldots,p) \tag{3.5}$$

The mode k is said to be uncontrollable from input i if $m_{ci}(k) = 0$. If $m_{oj}(k) = 0$, then mode k is unobservable from output j. A non minimal system is implied by zero residue. According to the aforementioned definitions, the relative controllability and observability measures for the i-th input and j-th output can be used to evaluate the controller performance for a particular mode. The sensitivity of the k-th eigenvalue to the gain K of a proportional feedback controller can be expressed such [38]:

$$\frac{\partial\lambda_k}{\partial K} = \|C\phi_k\psi_k B\| = \|R_k\| = \sigma_k \tag{3.6}$$

σ_k is the real part of the eigenvalues (λ_k) produced by the matrix A, where ($\lambda_k = \sigma_k \pm j\omega_k, k = 1,\ldots,n$). The residue, in this case, is the modal sensitivity of the constant gain controller. M. Traok [49] reported that the required mode shifting can be affected by information provided by residues about the magnitude of the feedback gains. He also founds that large gains are required to effect a shift fir a mode with low residue. The control input i has no influence on mode k response when $R_k(j,i)$ vanished if the feedback is based on the measured output signal j. Therefore, when chosing control loops or input/output pairs, large residues or joint controllability/observability measures are desirable. The joint controllability/observability measure is defined by [50]:

$$m_{cok}(i,j) = m_{ci}(k)m_{oj}(k) \tag{3.7}$$

Nonzero m_{cok} means that the mode k can be controlled using the input i and the output j. The signals u_i and y_j for which m_{cok} is maximum are the most efficient. If the maximum value of $m_{cok}(i,j)$ is obtained for i and j related with similar network component, then using decentral-

ized control will result in good damping for the mode k [50]. Global control design should be implemented if the maximum value of m_{cok} is obtained for i and j related with different network components.

I. Kamwa et. al, [42], found that the residue approach suffers a scaling problem when the output matrix C contains signals of widely varied physical significance, such as bus frequency (HZ), shaft speed (rad/s) and power flow over a transmission line (MW), simultaneously. All outputs must be of the same type to guarantee the validity of the relative measure. This shortcoming is overcome by introducing geometric measures [51]. The directional properties of particular column vectors in the power system matrices are used by the geometrical measures. They are used to study the strength of a stabilizing signal and a control site for a particular mode. The geometric attributes of controllability m_{ci} and observability m_{oj} related with the mode k are given by:

$$m_{ci}(k) = \cos(\alpha(\psi_k, b_i)) = \frac{|\psi_k b_i|}{\|\psi_k\|\|b_i\|} \tag{3.8}$$

$$m_{oj}(k) = \cos(\theta(\phi_k, c_j^T)) = \frac{|c_j \phi_k|}{\|\phi_k\|\|c_j\|} \tag{3.9}$$

with b_i represents the i-th column of B (corresponding to the ith input) and c_j the jth row of C (corresponding to the j-th output) [42]. $|z|, \|z\|$ are the modulus and Euclidean norm of z, respectively. $\alpha(\psi_k, b_i)$ is the geometrical angle between the input vector i and the k-th left eigenvector, while $\theta(\phi_k, c_j^T)$ is the geometric angle between the output vector j and the k-th right eigenvector. As shown from previous equations, the angle between the left eigenvectors and the columns of the input matrix B are used to find the controllability measure. Similarly, the angle between the right eigenvectors and the rows of the output matrix C are used to find the observability measure [42].

3.4 First Stage : System Identification

This section presents an (UIO) design for disturbance and fault estimations in power systems. The method results in three decoupled variations from the equations of a power system state space model; 1) fault and disturbance-free, 2) fault-dependent, 3) and disturbance-dependent. The first subsystem is not affected by the presence of faults or disturbances which affect power system operation. The second and third subsystems reflect power system operation which is

affected by the occurrence of fault and disturbances, respectively. The output measurements will be only used to find the state vectors of the second and third variations. This is done by choosing suitable coordinate transformations. UIO is then designed using the disturbance and fault-free subsystems. The magnitude and nature of faults and disturbances do not affect the estimation of the state vector by an UIO observer. As a result, the designed UIO is used for estimating faults and disturbances. The UIO design is based on the findings of T.-G. Park [41].

3.4.1 Unknown Input Observer (UIO) Design

Assuming that the power system state space model can be represented as:

$$\dot{x} = Ax + Bu + B_d d + B_f f \tag{3.10}$$

$$y = Cx \tag{3.11}$$

where $x \in \mathbb{R}^n$ contains all the states of the power system, $u \in \mathbb{R}^m$ is a control input vector, $d \in \mathbb{R}^l$ is a disturbance vector, $f \in \mathbb{R}^q$ is an actuator fault vector and $y \in \mathbb{R}^p$ is a measurement output vector. A, B, B_d, B_f and C are known real constant matrices of proper dimensions. An assumption is made at this stage which is related with the validity of the power system linear model upon and after the occurrence of faults and disturbances. It is assumed that $\text{rank}(C) = p$, $\text{rank}(B_d) = l$, $\text{rank}(B_f) = q$ and $\text{rank}([B_d \quad B_f]) = l + q$. It is also assumed that $\text{rank}(CB_d) = l, (p \geq l)$, $\text{rank}(CB_f) = q, (p \geq q)$ and $\text{rank}\,([CB_d \quad CB_f]) = l + q, (p \geq l + q)$. It is assumed, in what follows, that the sensors are perfectly reliable [41]. In addition, the UIO-based fault estimation is suitable for a linear system. The left pseudo-inverse of the matrix $X \in \mathbb{R}^{p \times (l+q)}$ is given by $X^\dagger = (X^T X)^{-1} X^T$, where $\text{rank}(X) = l + q$, $X^\dagger X = I_{l+q}$ and X^T is the transpose of X. Assuming that the $\text{rank}([CB_d \quad CB_f]) = l + q$, $[CB_d \quad CB_f]$ possesses $([CB_d \quad CB_f])^\dagger$. A square matrix P is used for a state coordinate transformation and is defined as [41]:

$$P = I_n - [B_d \quad B_f]([CB_d \quad CB_f])^\dagger C, \quad P \in \mathbb{R}^{n \times n} \tag{3.12}$$

The projector P satisfies $P^2 = P$. Assuming that $\text{rank}(B_d) = l$, $\text{rank}(B_f) = q$ and $\text{rank}([B_d \quad B_f]) = l + q$, a non-singular matrix can be found as:

$$T = [N \quad B_d \quad B_f], \quad N \in \mathbb{R}^{n \times (n-l-q)} \tag{3.13}$$

The matrix T is used for transforming the states of the given model (3.10) - (3.11) to new coordinates, where $N = PN_0$ and $N_0 \in \mathbb{R}^{n\times(n-l-q)}$ is a matrix which makes the matrix $[N_0 \quad B_d \quad B_f]$ non-singular. As a result, the system (3.10) - (3.11) can be rewritten as:

$$\dot{\bar{x}} = \overline{A}\bar{x} + \overline{B}u + \overline{B}_d d + \overline{B}_f f \tag{3.14}$$

$$y = \overline{C}\bar{x} \tag{3.15}$$

where

$$x = T\bar{x} = T\begin{bmatrix} \bar{x}_1 \\ \bar{x}_2 \\ \bar{x}_3 \end{bmatrix}, \quad \overline{A} = T^{-1}AT = \begin{bmatrix} \overline{A}_{11} & \overline{A}_{12} & \overline{A}_{13} \\ \overline{A}_{21} & \overline{A}_{22} & \overline{A}_{23} \\ \overline{A}_{31} & \overline{A}_{32} & \overline{A}_{33} \end{bmatrix}, \overline{B} = T^{-1}B = \begin{bmatrix} \overline{B}_1 \\ \overline{B}_2 \\ \overline{B}_3 \end{bmatrix}, \tag{3.16}$$

$$\overline{B}_d = T^{-1}B_d = \begin{bmatrix} 0 \\ I_l \\ 0 \end{bmatrix}, \overline{B}_f = T^{-1}B_f = \begin{bmatrix} 0 \\ 0 \\ I_q \end{bmatrix}, \overline{C} = CT = [CN \quad CB_d \quad CB_f] \tag{3.17}$$

with $\bar{x}_1 \in \mathbb{R}^{n-l-q}, \bar{x}_2 \in \mathbb{R}^l$ and $\bar{x}_3 \in \mathbb{R}^q$. It can be seen from (3.17) that the transformed disturbance and fault matrices, $\overline{B}_d$ and $\overline{B}_f$, don't affect the transformed state $\bar{x}_1$. The disturbance d and the fault f are directly contained in the differential equations related to $\bar{x}_2$ and $\bar{x}_3$ in (3.14). The disturbance and fault-free system can be expressed as:

$$\begin{bmatrix} I_{n-l-q} & 0 & 0 \end{bmatrix}\dot{\bar{x}} = \begin{bmatrix} \overline{A}_{11} & \overline{A}_{12} & \overline{A}_{13} \end{bmatrix}\bar{x} + \overline{B}_1 u \tag{3.18}$$

$$y = \begin{bmatrix} CN & CB_d & CB_f \end{bmatrix}\bar{x} \tag{3.19}$$

3.18 shows that $\dot{\bar{x}}_1$ is obtained only by the new transformed states $\bar{x}_1, \bar{x}_2$ and $\bar{x}_3$ in addition to the control input u. The output measurements y are only used to obtain $\bar{x}_2$ and $\bar{x}_3$, this is different from those expressed by $\bar{x}_1$ as well as y, this is further explained below.

The right pseudo inverse of $X \in \mathbb{R}^{(l+q)\times p}$ is given by $X^{\ddagger} = X^T(XX^T)^{-1}$ with the assumption that rank$([CB_d \quad CB_f]) = l+q$, $[CB_d \quad CB_f]^T$ possesses $([CB_d \quad CB_f]^T)^{\ddagger}$). A square matrix M is used for output transformation and is defined as [41]:

$$M = I_p - ([CB_d \quad CB_f]^T)^{\ddagger}[CB_d \quad CB_f]^T, \quad M \in R^{p\times p} \tag{3.20}$$

The projector matrix M satisfies $M^2 = M$. Assuming that rank(CB_d=l), rank($CB_f = q$ and rank($[CB_d \quad CB_f]$) $= l+q$, A non–singular matrix can be found as:

$$U = [CB_d \quad CB_f \quad Q], Q \in \mathbb{R}^{p\times(p-l-q)} \tag{3.21}$$

The matrix U is used for transforming the output of the power system model (3.19), where $Q = MQ_0$ and $Q_0 \in \mathbb{R}^{p\times(p-l-q)}$ is chosen such that $[CB_d \quad CB_F \quad Q_0]$ is a non-singular matrix. Let's define

$$U^{-1} = \begin{bmatrix} U_1 \\ U_2 \\ U_3 \end{bmatrix}, U_1 \in \mathbb{R}^{l\times p}, U_2 \in \mathbb{R}^{q\times p}, U_3 \in \mathbb{R}^{(p-l-q)\times p)} \tag{3.22}$$

gives:

$$U^{-1}U = \begin{bmatrix} U_1 \\ U_2 \\ U_3 \end{bmatrix} [CB_d \quad CB_f \quad Q] = \begin{bmatrix} U_1CB_d & U_1CB_f & U_1Q \\ U_2CB_d & U_2CB_f & U_2Q \\ U_3CB_d & U_3CB_f & U_3Q \end{bmatrix} = \begin{bmatrix} I_l & 0 & 0 \\ 0 & I_q & 0 \\ 0 & 0 & I_{p-l-q} \end{bmatrix} \tag{3.23}$$

Both sides of 3.19 are to be multiplied by U^{-1} while denoting 3.22 and 3.23, the new output coordinate system may be expressed as:

$$U_1y = U_1CN\bar{x}_1 + \bar{x}_2 \tag{3.24}$$

$$U_2y = U_2CN\bar{x}_1 + \bar{x}_3 \tag{3.25}$$

$$U_3y = U_3CN\bar{x}_1 \tag{3.26}$$

Let's assume that U is a non-singular matrix,$U^{-1} = U^{\dagger}$ can be expressed using partitioned matrices of $([CB_D \quad CB_f])^{\dagger}$ and $Q^{\dagger}$ as:

$$U^{-1} = \begin{bmatrix} U_1 \\ U_2 \\ \cdots \\ U_3 \end{bmatrix} = \begin{bmatrix} ([CB_d \quad CB_f])^{\dagger}) \\ \cdots \\ Q^{\dagger} \end{bmatrix} \tag{3.27}$$

It can be seen from (3.12),(3.13) and (3.27) that:

$$\begin{aligned}\begin{bmatrix} U_1 \\ U_2 \end{bmatrix} CN &= ([CB_d \quad CB_f])^{\dagger} CPN_0 \\ &= ([CB_d \quad CB_f])^{\dagger} \times C(I_n - [B_d \quad B_f]([CB_d \quad CB_f])^{\dagger} C)N_0 \\ &= (([CB_d \quad CB_f])^{\dagger} C - ([CB_d \quad CB_f])^{\dagger} \times [CB_d \quad CB_f]([CB_d \quad CB_f])^{\dagger} C)N_0 \\ &= (([CB_d \quad CB_f])^{\dagger} C - ([CB_d \quad CB_f])^{\dagger} C)N_0 \\ &= 0_{(l+q)\times(n-l-q)} \end{aligned} \tag{3.28}$$

(3.24), (3.25) and (3.26) can be simplified into:

$$U_1 y = \bar{x}_2 \tag{3.29}$$

$$U_2 y = \bar{x}_3 \tag{3.30}$$

$$U_3 y = U_3 CN \bar{x}_1 \tag{3.31}$$

It is noticed that $\bar{x}_2$ and $\bar{x}_3$ are realized by only output measurements. $U_1CN = 0$ and $U_2CN = 0$ are obtained after using the projectors (3.12) and (3.20) in finding the transformation matrices (3.13) and (3.21). As a result, a more simplified order model is obtained as (3.32) and (3.33) below. By substituting (3.29) and (3.30) into (3.18) and combining it with (3.31), the following is obtained:

$$\dot{\bar{x}}_1 = \overline{A}_{11}\bar{x}_1 + \overline{B}_1 u + E_1 y \tag{3.32}$$

$$\bar{y} = \overline{C}_1 \bar{x}_1 \tag{3.33}$$

where $E_1 = \overline{A}_{12}U_1 + \overline{A}_{13}U_2$, $\overline{C}_1 = U_3CN$ and $\bar{y} = U_3 y$. Assuming that the pair $(\overline{A}_{11}, \overline{C}_1)$ is observable or detectable, a UIO can be designed for the system (3.32) and (3.33) as:

$$\begin{aligned}\dot{\hat{\bar{x}}}_1 &= ((\overline{A}_{11} - L\overline{C}_1)\hat{\bar{x}}_1 + \overline{B}_1 u + L\bar{y} + E_1 y \\ &= ((\overline{A}_{11} - L\overline{C}_1)\hat{\bar{x}}_1 + \overline{B}_1 u + L^* y \end{aligned} \tag{3.34}$$

where $\hat{\bar{x}}_1 \in \mathbb{R}^{n-l-q}$ and $L^* = LU_3 + E_1$. The matrix $L \in \mathbb{R}^{(n-l-q)\times(p-l-q)}$ is the observer gain which makes the matrix $\overline{A}_{11} - L\overline{C}_1$ stable. The error dynamics related with estimating the state

$\bar{x}_1$ from (3.32) and (3.34) may be expressed as:

$$\dot{e}_{\bar{x}_1} = (\overline{A}_{11} - L\overline{C}_1)e_{\bar{x}_1} \tag{3.35}$$

where $e_{\bar{x}_1} = \hat{\bar{x}}_1 - \bar{x}_1$. The error will converge exponentially to zero if $(\overline{A}_{11} - L\overline{C}_1)$ is Hurwitz. The state of the given system (3.10) and (3.11) can also be estimated from (3.29) and (3.30) as [41]:

$$\hat{x} = T\hat{\bar{x}} = T\begin{bmatrix} \hat{\bar{x}}_1 \\ \hat{\bar{x}}_2 \\ \hat{\bar{x}}_3 \end{bmatrix} = T\begin{bmatrix} \hat{\bar{x}}_1 \\ U_1 y \\ U_2 y \end{bmatrix} \tag{3.36}$$

The estimates of the fault f and the disturbance d may be found once having an estimate of $\bar{x}_1$ from the UIO described in (3.34). A fault estimate $\hat{f} \in \mathbb{R}^q$ can be obtained from the differential equations of the state vector $\bar{x}_3$ in (3.14) as [41]:

$$\begin{aligned} \hat{f} &= \dot{\hat{\bar{x}}}_3 - [\overline{A}_{31} \quad \overline{A}_{32} \quad \overline{A}_{33}]\hat{\bar{x}} - \overline{B}_3 u \\ &= U_2\dot{y} - \overline{A}_{31}\hat{\bar{x}}_1 - (\overline{A}_{32}U_1 + \overline{A}_{33}U_2)y - \overline{B}_3 u \end{aligned} \tag{3.37}$$

The fault estimation error vector from (3.14), (3.15), (3.14), (3.15),(3.18), (3.36) and (3.37) is given by [41]:

$$e_f = \overline{A}_{31} e_{\bar{x}_1} \tag{3.38}$$

Similarly, a disturbance estimate $\hat{d} \in \mathbb{R}^l$ may be obtained from the differential equations corresponding to the state vector $\bar{x}_2$ in (3.14) as:

$$\begin{aligned} \hat{d} &= \dot{\hat{\bar{x}}}_2 - [\overline{A}_{21} \quad \overline{A}_{22}\overline{A}_{23}]\hat{\bar{x}} - \overline{B}_2 u \\ &= U_1\dot{y} - \overline{A}_{21}\hat{\bar{x}}_1 - (\overline{A}_{22}U_1 + \overline{A}_{23}U_2)y - \overline{B}_2 u \end{aligned} \tag{3.39}$$

The disturbance estimation error is found using (3.14), (3.15), (3.29), (3.30), (3.31), (3.36) and (3.39) as [41]:

$$e_d = \overline{A}_{21} e_{\bar{x}_1} \tag{3.40}$$

where

$$e_d = d - \hat{d}$$

3.5 Second Stage : Robust Control Design

3.5.1 Singular Values and Singular Vectors

In the previous sections, eigenvalues were adopted to evaluate the small signal stability of a power system. The modal behavior of a system can be well understood using eigenvalue analysis. However, useful meanings of generalizing gain $|G(j\omega)|$ of a system cannot be provided by their magnitudes. On the other hand, a good measure is obtained by the singular values for the size of the system. In addition, indications of strong/weak input or output directions could be inferred by the corresponding singular vectors. Singular Value Decomposition (SVD) may be defined as [5]:

Let $A \in \mathbb{F}^{m\times n}$. Unitary matrices can be found as:

$$U = [u_1, u_2, \ldots, u_m] \in \mathbb{F}^{m\times m} \tag{3.41}$$

$$V = [v_1.v_2, \ldots, v_n] \in \mathbb{F}^{n\times n} \tag{3.42}$$

such that:

$$A = U\Sigma V^*, \qquad \Sigma = \begin{bmatrix} \Sigma_1 & 0 \\ 0 & 0 \end{bmatrix} \tag{3.43}$$

where,

$$\Sigma_1 = \begin{bmatrix} \sigma_1 & 0 & \ldots & 0 \\ 0 & \sigma_2 & \ldots & 0 \\ \vdots & \vdots & \ddots & \vdots \\ 0 & 0 & \ldots & \sigma_p \end{bmatrix} \tag{3.44}$$

and,

$$\sigma_1 \geq \sigma_2 \geq \ldots \sigma_p \geq 0, p = min\{m,n\} \tag{3.45}$$

The singular values can be geometrically interpreted as the lengths of the semi-axis of the hyperellipsoid E given by:

$$E = \{y : y = Ax, x \in \mathbb{C}^n, \|x\| = 1\} \tag{3.46}$$

For all $\|x\| = 1$, v_1 represents the direction in which $\|y\|$ is the largest, where v_n represents the direction in which $\|y\|$ is the smallest. $v_1(v_n)$ is the highest (lowest) gain input (or control)

direction, while $u_1(u_m)$ is the highest (lowest) gain output (or observing) direction from the input/output point of view. σ_i connects these input and output directions. Since $\|u_i\|_2 = 1$ and $\|v_i\|_2 = 1$, it is seen that the gain of the matrix in this direction is given by σ_i. This can be stated as follows:

$$\sigma_i(A) = \|Av_i\|_2 = \frac{\|Av_i\|_2}{\|v_i\|_2} \tag{3.47}$$

As mentioned previously, better information is given about the gains of the plant by singular values. They are also applicable to non-square plants. In addition, input and output directions are given by singular vectors which are orthogonal. Maximum and minimum singular values can also be defined as the largest and smallest singular value of a matrix. They are given as:

$$\overline{\sigma}(A) = \sigma_1(A) = max\frac{\|Ad\|_2}{\|d\|_2} = \frac{\|Av_1\|_2}{\|v_1\|_2}, \qquad d \neq 0 \tag{3.48}$$

$$\underline{\sigma} = \sigma_p = min\frac{\|Ad\|_2}{\|d\|_2} = \frac{\|Av_k\|_2}{\|v_k\|_2}, \qquad d \neq 0 \tag{3.49}$$

The ratio of maximum singular value to minimum singular value is called the condition number of the plant. It is given by:

$$\gamma(G) = \frac{\overline{\sigma}(G)}{\underline{\sigma}(G)} \tag{3.50}$$

An important frequency domain property of a power system model is the condition number. It gives an indication about the degree of difficulty to control it. A large condition number means usually that the plant is ill-conditioned and is difficult to control.

3.5.2 H_∞ and H_2 Norm

In this section, vector and matrix norms used in the will be defined. Let $G(s)$ be the power system transfer function of a stable single input single output (SISO) LTI-system of input $u(t)$ and output $y(t)$. $G(s)$ is the Laplace transform of the impulse response $g(t)$ of the system, the $\mathbf{H}_2$ norm of $G(s)$ is defined as [8]:

$$\|G\|_2 = (\int_0^\infty g(t)^2 \mathrm{d}t)^{1/2} \tag{3.51}$$

The previous norm is defined for a particular input signal which is the Dirac impulse $\delta(t)$. According to Parseval's theorem the $\mathbf{H}_2$ norm is defined in the frequency domain as follows:

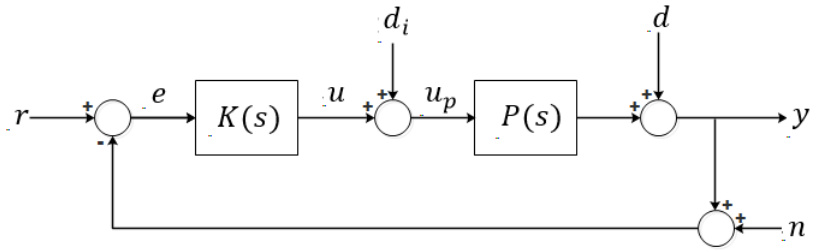

Figure 3.2: Standard feedback configuration [5]

$$\|G\|_2 = (\frac{1}{2\pi}\int_{-\infty}^{+\infty} |G(j\omega)|^2 \mathrm{d}\omega)^{1/2} \tag{3.52}$$

It can be seen from (3.52) that the $\mathbf{H}_2$-norm represents the average system gain taken over all frequencies [52]. The gain provided by the system can be defined for a given particular input as the ratio of the $\mathbf{L}_2$-norm of the output signal to the $\mathbf{L}_2$-norm of the input signal $\|G\|_{gain} = \frac{\|Gu\|_2}{\|u\|_2}$, with $\|u\|_2 \neq 0$. An alternative approach for evaluating the $\mathbf{L}_2$-gain for a particular input, one can also determine the greatest possible $\mathbf{L}_2$-gain over the set of square integral signals. This is the definition of the $\mathbf{H}_\infty$-norm of a system, which can be expressed as:

$$\|G\|_\infty = sup\frac{\|Gu\|_2}{\|u\|_2}, \quad u \in \mathbf{L}_2 \quad and \quad \|u|_2 \neq 0 \tag{3.53}$$

In the frequency domain, the $\mathbf{H}_\infty$-norm of a power system is the maximum value of that transfer function over the complete frequency range. It is taken as the peak value of the maximum singular value response as function of frequency and expressed as:

$$\|G(s)\|_\infty = max\{\overline{\sigma}(G(j\omega))\} \quad \forall\omega \tag{3.54}$$

3.5.3 Performance and Stability Requirements

The properties of a feedback system is discussed in this section. In particular, the benefit of the feedback structure is considered in addition to the tradeoffs faced by control engineers for conflicting control objectives. This is articulated on achieving the advantages of feedback structure against the different types of uncertainties. Fig.3.2 shows a feedback system, $K(s)$ is the controller transfer matrix and $P(s)$ is the power system transfer function; r, y, d_i, d, n and e denotes the reference, output, input and output disturbances,measurement noise and tracking error signal vectors, respectively [5]. The closed loop system is internally stable if the following

equations are satisfied [5]:

$$y = PK(I+PK)^{-1}(r-n)+(I+PK)^{-1}Pd_i+(I+PK)^{-1}d \tag{3.55}$$

$$e = (I+PK)^{-1}(r-d)+PK(I+PK)^{-1}n-(I+PK)^{-1}Pd_i \tag{3.56}$$

$$u = K(I+PK)^{-1}(r-n)-K(I+PK)^{-1}d-KP(I+KP)^{-1}d_i \tag{3.57}$$

$$u_p = K(I+PK)^{-1}(r-n)-K(I+PK)^{-1}d+(I+KP)^{-1}d_i \tag{3.58}$$

In (3.55), the transfer function which maps d to y is called the output sensitivity function (S_o) and is defined as:

$$S_o = (I+PK)^{-1}, \quad y = S_o d \tag{3.59}$$

In addition, the output complementary sensitivity function (T_o) is defined as:

$$T_o = I - S_o = PK(I+PK)^{-1} \tag{3.60}$$

The fundamental advantages and control design objectives contained in feedback loops are described by these four equations, for example:

1. Making S_o small will reduce the effects of disturbance d on the plant output, as can be seen from equation (3.15). Frequency-dependent singular values measured as $\overline{\sigma}(S_o(j\omega))$ can be used to indicate the magnitude of S_o in a certain range of frequencies.

2. The effects of measurement noise on the output signal can be reduced by making the complementary sensitivity measured as $\overline{\sigma}(T_o(j\omega))$ small over the frequency range of the measurement noise.

As a result, the requirements on the sensitivity and/or complementary sensitivity functions can be used to specify the design objectives of a feedback control system. Other closed-loop transfer functions can be also utilized. Appropriate weighting functions can be chosen to achieve the control design objectives. For example, the performance of S_o and T_o can be expressed as:

$$\overline{\sigma}(W_1(j\omega)S_o(j\omega)) \leq 1 \tag{3.61}$$

$$\overline{\sigma}(W_2(j\omega)T_o(j\omega)) \leq 1 \tag{3.62}$$

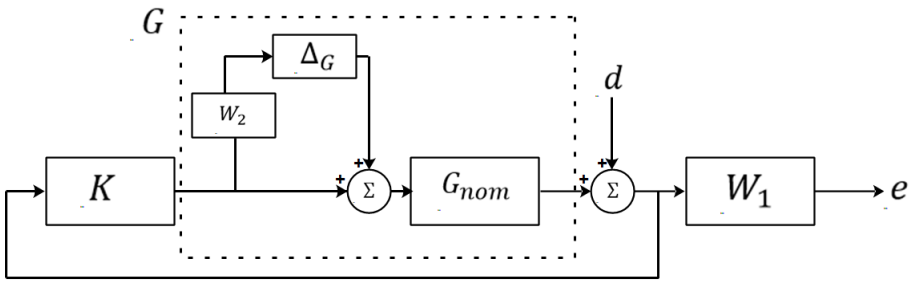

Figure 3.3: Robust stability and performance objectives [6]

where performance objectives are approximated by gains of the transfer functions $W_1(s)$ and $W_2(s)$ in the frequency domain. Conditions for robust stability, nominal performance and robust performance can be derived for Fig.3.3 as [6]:

1. **Nominal Performance** is achieved by the closed-loop system if the following condition is satisfied for the nominal power system model, G_{nom}. This is equivalent to:

$$\text{Nominal Performance} \Leftrightarrow \|W_1(I+G_{nom}K)^{-1}\|_\infty < 1 \tag{3.63}$$

2. **Robust Stability** is achieved if, for all the possible plant models $G \in Y$, the closed loop system is internally stable . This may be written as:

$$\text{Robust Stability} \Leftrightarrow \|W_2KG_{nom}(I+KG_{nom})^{-1}\|_\infty < 1 \tag{3.64}$$

3. **Robust Performance** is achieved if, for all $G \in Y$, the closed-loop system is internally stable. In addition, the following condition must be satisfied for every $G \in Y$.

$$\|W_1(I+GK)^{-1}\|_\infty < 1 \tag{3.65}$$

where $Y := \{G_{nom}(I+\Delta_G W_2) : \Delta_G \quad \text{stable}, \quad \|\Delta_G\|_\infty \leq 1\}$, the unknown transfer function $\Delta_G(s)$ is used to parametrize the potential differences between the nominal model $G_{nom}(s)$, and the actual behavior of the real plant, denoted by G.

3.5.4 Standard H_∞ Robust Control Design

The H_∞ control problem can often be conventionally formulated as one of disturbance rejection. Specifically, it consists of minimizing the close-loop root mean squares (RMS, the largest gain

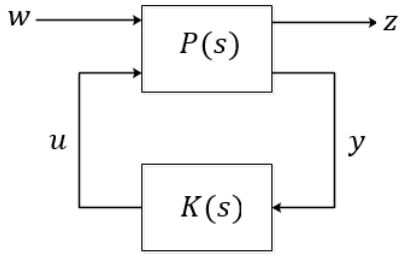

Figure 3.4: Robust control design [7]

over all square-integrable inputs) gain from w to z as in Fig.3.4. This objective can be stated as to minimize the impact of the worst-case disturbance w on the output z. Fig. 3.4 consists of an augmented plant $P(s)$ which includes the weighting functions and a controller $K(s)$ which is obtained by solving the standard H_∞ problem [53]. The plant inputs are divided as [53]:

- u represents the control input vector;
- w represents the exogenous input vector.

The plant outputs categorized as follows [53]:

- y represents the measurement variables vector which are used as the input vector of the controller to provide the control stabilizing signal u.
- z represents the regulated variables vector which are used in evaluating the performance of the closed loop system.

The augmented plant $P(s)$ may be represented as [7]:

$$\begin{pmatrix} Z(s) \\ Y(s) \end{pmatrix} = \begin{pmatrix} P_{11}(s) & P_{12}(s) \\ P_{21}(s) & P_{22}(s) \end{pmatrix} \begin{pmatrix} W(s) \\ U(s) \end{pmatrix} \tag{3.66}$$

where $U(s) = K(s)Y(s)$. The closed-loop transfer function from w to z is given by the linear-fractional expression $F_\ell(P,K)$ such that $Z(s) = F_\ell(P,K)W(s)$, where

$$F_\ell(P,K) = P_{11} + P_{12}K(I - P_{22}K)^{-1}P_{21} \tag{3.67}$$

The power system plant P(s) can also be written in the state-space realization as:

$$\dot{x} = Ax + B_1 w + B_2 u \tag{3.68}$$

$$z = C_1 x + D_{11} w + D_{12} u \tag{3.69}$$

$$y = C_2 x + D_{21} w + D_{22} u \tag{3.70}$$

which results in a packed notation of,

$$P(s) = \left[\begin{array}{c|cc} A & B_1 & B_2 \\ \hline C_1 & D_{11} & D_{12} \\ C_2 & D_{21} & D_{22} \end{array}\right]$$

where [54],

x : state variable (e.g. machine speed, bus voltage)

w : disturbance input variable (e.g. a step variation in governor turbine reference power)

u : control input variable (e.g. output of FACTS controllers)

y : measured output variable (e.g. bus voltage, line current, power flow)

z : regulated output variable

The optimal H_∞ control can be summarized as follows [7]:

"Find an internally stabilizing and realizable controller K(s) for a given plant P(s) such that the H_∞ norm of the linear fractional expression $F_\ell(P,K)$ is below a given level γ.

i.e. $\|F_\ell(P,K)\|_\infty < \gamma$; with $\gamma \in \mathbb{R}$ and $\gamma > 0$".

3.5.5 Formulation of Weighted Mixed-sensitivity H_∞ Robust Control

Mixed-sensitivity is defined as the transfer function shaping problem. It shapes the sensitivity function $S = (I + GK)^{-1}$ with one or more other closed-loop transfer functions like KS or the complementary sensitivity transfer function $T = I - S$. Fig.3.5 shows a standard control configuration for the S/KS mixed-sensitivity optimization. A tracking problem is considered here. The exogenous input is a reference command, r, and the error signals are $z_1 = W_1 e$ and $z_2 = W_2 u$. In this tracking problem, it can be seen that $z_1 = W_1 S w$ and $z_2 = W_2 KS w$. W_1 is the weighting on tracking error and W_2 is the weighting on the control signal. The elements of the generalized

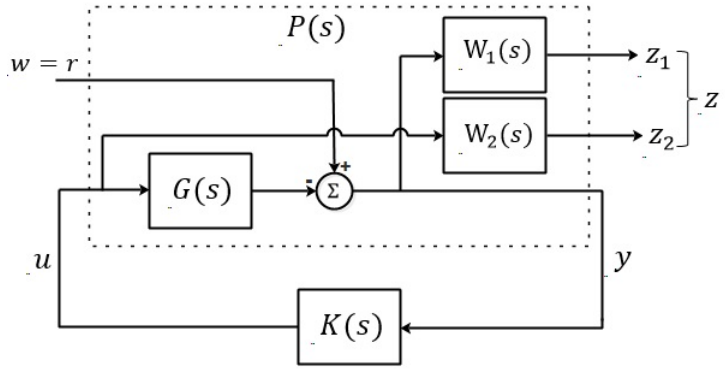

Figure 3.5: S/KS mixed-sensitivity minimization in standard form [8]

plant P as [8]:

$$P_{11} = \begin{bmatrix} W_1 \\ 0 \end{bmatrix}, \quad P_{12} = \begin{bmatrix} -W_1 G \\ W_2 \end{bmatrix}, \quad P_{21} = I, \quad P_{22} = -G \tag{3.71}$$

where the partitioning is:

$$\begin{bmatrix} z \\ y \end{bmatrix} = \begin{bmatrix} P_{11} & P_{12} \\ P_{21} & P_{22} \end{bmatrix} \begin{bmatrix} w \\ u \end{bmatrix} \tag{3.72}$$

and,

$$F_\ell(P,K) = \begin{bmatrix} W_1 S \\ W_2 KS \end{bmatrix} \tag{3.73}$$

The H_∞ optimal control problem seeks to find all stabilizing controllers K which minimize the weighted mixed-sensitivity transfer function:

$$\left\| \begin{bmatrix} W_1 S \\ W_2 KS \end{bmatrix} \right\|_\infty \tag{3.74}$$

The bandwidth requirements on closed-loop transfer functions can be reflected by choosing appropriate weighting functions. Stable high-pass and low-pass filters are adequate to perform the needed shaping and trade-offs. The shaping design would minimize a weighted mix of the sensitivity function S that ensures good reference tracking and disturbance rejection and control sensitivity functions KS which reflects the robustness issues and constraints the controller effort. The selection of the weighting matrices $W_1(s)$ and $W_2(s)$ represents an important step in the control design process. Knowledge about the dynamic behavior of power system is required

for proper choice of the weighting functions in order to achieve the control design objectives (stability and performance requirements). Many iterations and fine tuning may be required during the design of weighting functions for a particular design problem. As a result, it is difficult to obtain a general formula for weighting functions design.

3.5.6 LMI Approach to Multi-Objective H_∞ Synthesis

A *linear matrix inequality (LMI)* is given by an expression of the following form [7]:

$$F(x) = F_0 + x_1F_1 + \ldots + x_mF_m < 0 \tag{3.75}$$

where,

- $x = (x_1, \ldots, x_N)$ is the scale variables vector to be found. Its also referred as the decision variables or the optimization variables
- $F_0, \ldots, F_m$ are real symmetric matrices, i.e. $F_i = F_i^T \in \mathbb{R}^{n\times n}$
- < 0 means "negative definite", i.e. $u^TF(x)u < 0$ for all $u \in \mathbb{R}^n, u \neq 0$.

An example of a LMI which arises in control applications is the Lyapunov inequality and can be written as:

$$A^TX + XA < 0 \tag{3.76}$$

The LMI (3.75) is a convex constraint on the decision variable(x). The solution, if it exists, to (3.75) is said to fall under a convex optimization problem. There are three generic optimization problems that can be solved in LMI framework which are feasibility problem, linear objective optimization and generalized eigenvalue minimization problem. These problems can be stated as follows [7]

- **Feasibility problem**

  To find $x \in \mathbb{R}^N$ that satisfies the LMI system $A(x) < B(x)$.

- **Minimization of a linear objective under LMI constraints**

  To minimize c^Tx over $x \in \mathbb{R}^N$ subject to $A(x) < B(x)$

- **Generalized eigenvalue minimization problem**

  To minimize γ over $x \in \mathbb{R}^N$ subject to

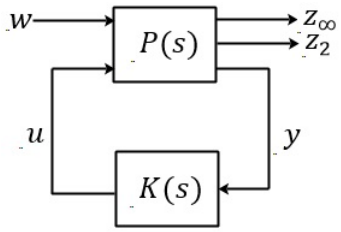

Figure 3.6: Multi-objective H_∞ synthesis [7]

$C(x) < D(x)$

$0 < B(x)$

$A(x) < \gamma B(x)$

A state-space realization for the plant P is needed to formulate the LMI problem, in this thesis, the generalized realization of (3.68) - (3.70) is adopted to solve for a stabilizing controller using the LMI approach. Standard H_∞ synthesis cannot sufficiently represent all control design objectives in may applications. For example, the Linear Quadratic Gaussian (LQG) terms are used to more naturally express noise attenuation against random disturbances. In addition, direct placement of the closed-loop poles in a pre-specified region is not allowed by the pure H_∞ synthesis. Accordingly, multi-objective synthesis is highly desirable in practice and LMI framework offers powerful tools to tackle such problems [55]. The LMI solving techniques address different examples of multi-objective design. An example is the mixed H_2/H_∞ design with regional pole placement. Fig.3.6 shows the control problem. The H_∞ performance is associated with the output channel z_∞ and the LQG aspects(H_2 performance) is associated with z_2. $T_\infty(s)$ and $T_2(s)$ denote the closed-loop transfer functions from w to z_∞ and z_2 , respectively.The multi-objective synthesis problem can stated as follows:
Design an output-feedback controller $u = K(s)y$ that [7]:

- Maintains the H_∞ norm of $T_\infty(s)$(RMS gain) below some prescribed value $\gamma_0 > 0$
- Maintains the H_2 norm of $T_2(s)$(LQG cost) below some prescribed value $v_0 > 0$
- Minimizes a trade-off criterion of the form $\alpha\|T_\infty\|_\infty^2 + \beta\|T_2\|_2^2$ with $\alpha > 0$ and $\beta \geq 0$
- Places the closed-loop poles in some prescribed LMI region D

LMI Formulation

Assuming that,

$$\dot{x} = Ax + B_1 w + B_2 u \tag{3.77}$$

$$z_\infty = C_\infty x + D_{\infty 1} w + D_{\infty 2} u \tag{3.78}$$

$$z_2 = C_2 x + D_{21} w + D_{22} u \tag{3.79}$$

$$y = C_y x + D_{y1} w \tag{3.80}$$

and,

$$\dot{x}_k = A_k x_k + B_k y \tag{3.81}$$

$$u = C_k x_k + D_k y \tag{3.82}$$

be the state-space representation of the power system model $P(s)$ and controller $K(s)$, respectively. In addition, assume that:

$$\dot{x} = A_{cl} x_{cl} + B_{cl} w \tag{3.83}$$

$$z_\infty = C_{cl1} x_{cl} + D_{cl1} w \tag{3.84}$$

$$z_2 = C_{cl2} x_{cl} + D_{cl2} w \tag{3.85}$$

be the associated state space equations of the closed-loop system. The control design objectives can be summarized as [56]:

- H_∞ **perfromance:** the closed-loop *RMS* gain from w to z_∞ does not exceed γ if and only if there exists a symmetric matrix X_∞ such that [7]:

$$\begin{pmatrix} A_{cl}X_\infty + X_\infty A_{cl}^T & B_{cl} & X_\infty C_{cl1}^T \\ B_{cl}^T & -I & D_{cl1}^T \\ C_{cl1}X_\infty & D_{cl1} & -\gamma^2 I \end{pmatrix} < 0 \tag{3.86}$$

- H_2 **performance:** the H_2 norm of the closed-loop transfer function from w to z_2 does not exceed v if and only if $D_{cl2} = 0$ and there exist two symmetric matrices X_2 and Q such

that [7]:

$$\begin{pmatrix} A_{cl}X_2 + X_2A_{cl}^T & B_{cl} \\ B_{cl}^T & -I \end{pmatrix} < 0 \tag{3.87}$$

$$\begin{pmatrix} Q & C_{cl2}X_2 \\ X_2C_{cl2}^T & X_2 \end{pmatrix} > 0 \tag{3.88}$$

$$Trace(Q) < v^2 \tag{3.89}$$

- **Pole placement:** the closed-loop poles lie in the LMI region [7]:

$$D = z \in \mathbf{C} : L + Mz + M^T\bar{z} < 0 \tag{3.90}$$

with $L = L^T = [\lambda_{ij}]_{1\leq i,j\leq m}$ and $M = [\mu_{ij}]_{1\leq i,j\leq m}$ if and only if there exists a symmetric matrix X_{pol} satisfying

$$[\lambda_{ij}X_{pol} + \mu_{ij}A_{cl}X_{pol} + \mu_{ji}X_{pol}A_{cl}^T]_{1\leq i,j\leq m} < 0, X_{pol} > 0 \tag{3.91}$$

A single Lyapunov matrix must be sought for tractability in the LMI framework, so let $X := X_\infty = X_2 = X_{pol}$. As a result, the three sets of constraints are enforced. Factorizing X as $X = X_1X_2^{-1}, X_1 = \begin{pmatrix} R & I \\ M^T & 0 \end{pmatrix}, X_2 = \begin{pmatrix} 0 & S \\ I & N^T \end{pmatrix}$ The controller variables are changes as:

$$A_K = NA_kM^T + NB_kC_yR + SB_2C_KM^T + S(A + B_2D_kC_y)R \tag{3.92}$$

$$B_K = NB_k + SB_2D_k \tag{3.93}$$

$$C_K = C_kM^T + D_kC_yR \tag{3.94}$$

$$D_K = D_k \tag{3.95}$$

The inequality constraints on X are readily turned into LMI constraints in the variables R, S, Q, A_K, B_K, C_K and D_K [7]. This leads to the following suboptimal LMI formulation of the multi-objective syn-

thesis problem: Minimize $\alpha\gamma^2+\beta$Trace(Q) over R,S,Q,A_K,B_K,C_K,D_K, and γ^2 satisfying [7]:

$$\begin{pmatrix} AR+RA^T+B_2C_K+C_K^TB_2^T & A_K^T+A+B_2D_KC_y & B_1+B_2D_KD_{y1} & (C_\infty R+D_{\infty 2}C_K)^T \\ A_K+(A+B_2D_KC_y)^T & A^TS+SA+B_K+C_y^TB_K^T & SB_1+B_KD_{y1} & C_\infty^T+C_y^TD_K^TD_{\infty 2}^T \\ (B_1+B_2D_KD_{y1})^T & SB_1+B_KD_{y1} & -I & (D_{\infty 1}+D_{\infty 2}D_KD_{y1})^T \\ C_\infty R+D_{\infty 2}C_K & C_\infty+D_{\infty 2}D_KC_y & D_{\infty 1}+D_{\infty 2}D_KD_{y1} & -\gamma^2 I \end{pmatrix} <0 \quad (3.96)$$

$$\begin{pmatrix} Q & C_2R+D_{22}C_K & C_2+D_{22}D_KC_y \\ (C_2R+D_{22}C_K)^T & R & I \\ (C_2+D_{22}D_KC_y)^T & I & S \end{pmatrix} > 0 \quad (3.97)$$

$$\left[\lambda_{ij}\begin{pmatrix} R & I \\ I & S \end{pmatrix}+\mu_{ij}\begin{pmatrix} AR+B_2C_K & A+B_2D_KC_y \\ A_K & SA+B_KC_y \end{pmatrix}+\mu_{ji}\begin{pmatrix} RA^T+C_K^TB_2^T & A_K^T \\ (A+B_2D_KC_y)^T & A^TS+C_y^TB_K^T \end{pmatrix}\right]_{1\le i,j\le m} < 0 \quad (3.98)$$

$$Trace(Q) < v_0^2 \quad (3.99)$$

$$\gamma^2 < \gamma_0^2 \quad (3.100)$$

$$D_{21}+D_{22}D_KD_{y1}=0 \quad (3.101)$$

The limits of closed-loop H_∞ and H_2 performances can be given after finding the solutions γ^*, Q^* of this LMI problem as:

$$\|T_\infty\|_\infty \le \gamma^* \quad (3.102)$$

$$\|T_2\|_2 \le \sqrt{Trace(Q^*)} \quad (3.103)$$

4

CASE STUDIES

4.1 Single Machine to Infinite Bus System (SMIB)

Fig.4.1 shows a single machine connected to a strong grid through transmission lines. Appendix *A* gives a detailed model descriptions of the system. For the purpose of the analysis, the grid is reduced by finding the Thevenin's equivalent reactance of the transmission lines connected to the machine. The dynamics associated with the machine had little impact on the voltage and frequency of Thevenin's voltage due to the relative size of the system to which the machine was supplying power. An infinite bus refers to a constant voltage source and constant frequency [2].

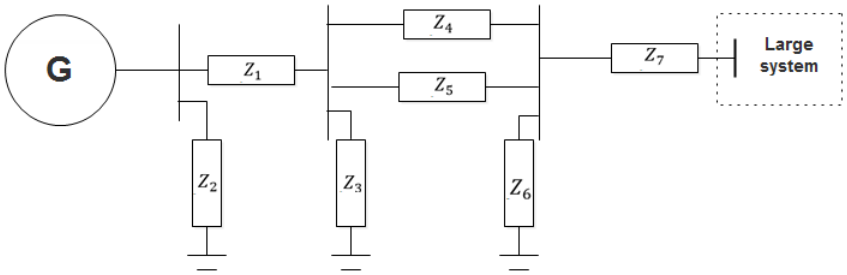

Figure 4.1: Single line diagram - Single machine to a large system

4.1.1 Full-order Model and Small Signal Analysis

The nonlinear model of this system was developed following the same terminology used in [2]. A subtransient model with four coils on the rotor is used to represent all generators. There are one field and one equivalent damper coil in the direct-axis in addition to two damper coils in the quadrature-axis. The generator is equipped with a static exciter with $G_{ex}(s) = K_A$, where $G_{ex}(s)$ is the transfer function associated with the AVR and exciter system. In addition, the power system stabilizer (PSS) consists of three blocks: a phase compensation block, a signal washout block and a gain block as shown in Fig. 2.3. As a result,the generator has 9 states as described previously in Chapter 2. The nominal plant is selected based on an output power of 1998 MW. This operating point is chosen to reflect stressed power system operation. The base units for this system are chosen such 2220 MVA and 24 kV. The values used to model the static exciter with AVR and PSS are; $K_A = 200, T_R = 0.02s, K_{STAB} = 9.5, T_W = 1.4s, T_1 = 0.154s$ and $T_2 = 0.033s$. This operating point was used to linearize the nonlinear model. The following eigenvalues are obtained when the generator is equipped with a static exciter only:

$$\lambda_1, \lambda_2 = 0.53 \pm j7.38 \quad (\omega_d = 1.17Hz, \zeta = -0.07)$$

$$\lambda_3, \lambda_4 = -17.6 \pm j11.4 \quad (\omega_d = 1.81Hz, \zeta = 0.84)$$

$$\lambda_5 = -24.8, \lambda_6 = -1.97, \lambda_7 = -54.4$$

The eigenvalues show two local modes of oscillations which have frequency of 1.17 and 1.81 Hz and damping ratio of -0.07 and 0.84, respectively. The first local mode is unstable and is expected to grow in magnitude when small disturbance affects the system. No inter-area oscillations are observed. Table 4.1 illustrates the impact of introducing PSS to the system and varying the stabilizer gain K_{STAB}. It is seen that the PSS successfully shifts the unstable eigenvalues to the left-half plane of the complex coordinates at stabilizer gains K_{STAB} greater than 5.0. It is also noticed that as K_{STAB} is increased, the frequency slightly decreases and the rotor angle mode damping increases. The reduction in frequency indicates that the synchronizing torque is reduced; this is caused by the PSS phase lead circuit which provides overcompensation at frequency of rotor oscillation.

Table 4.1: The effect of varying the stabilizer gain K_{STAB}, with $K_A = 200$

	Eigenvalues						
K_{STAB}	λ_1, λ_2	λ_3, λ_4	λ_5	λ_6	λ_7	λ_8	λ_9
0.1	$0.51 \pm j7.4$	$-17.6 \pm j11.4$	-24.9	-1.97	-54.4	-30.4	-0.71
1.0	$0.34 \pm j7.4$	$-17.1 \pm j11.8$	-24.9	-1.97	-54.4	-30.9	-0.72
5.0	$-0.37 \pm j7.2$	$-15.4 \pm j13.6$	-24.9	-1.97	-54.5	-32.8	-0.73
9.5	$-1.08 \pm j6.8$	$-13.9 \pm j15.5$	-25.0	-1.96	-54.5	-34.3	-0.74
15.0	$-1.75 \pm j6.2$	$-12.5 \pm j17.7$	-25.0	-1.95	-54.6	-35.6	-0.76
Dominant States	$\Delta\omega_r, \Delta\delta$	$\Delta\psi_{fd}, \Delta\psi_{1d}$	$\Delta\psi_{2q}$	$\Delta\psi_{1q}$	Δv_1	Δv_2	Δv_s

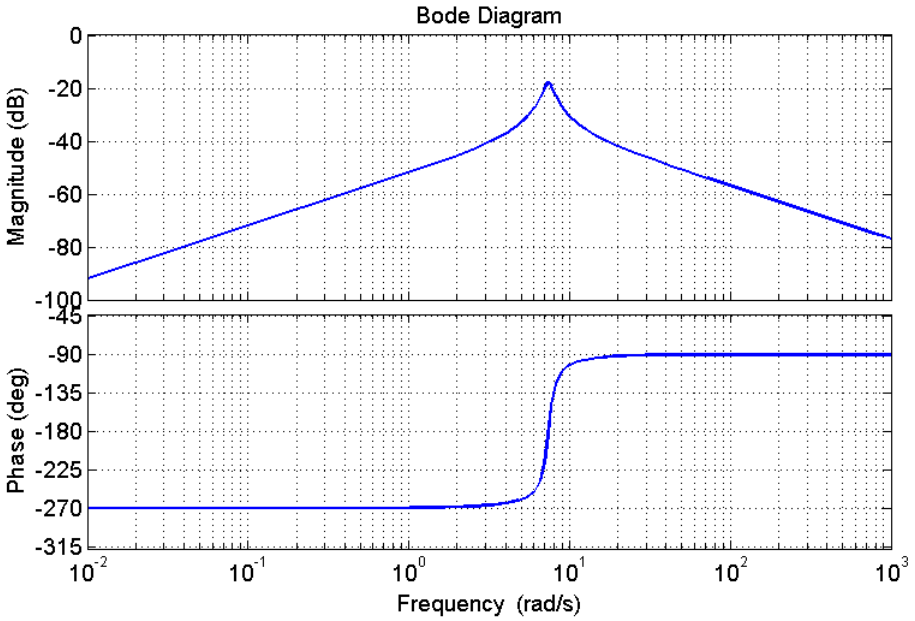

Figure 4.2: Frequency response of rotor angular speed (Single machine to infinite bus)

4.1.2 Selection of Measurements and Control Site Locations

Residual analysis are used to study the strength of candidate stabilizing signals.Table4.2 shows the residue related with the different local signals. Measurements can be only taken for rotor speed and exciter voltage and thus the exciter voltage is used for robust control design.

Table 4.2: Residual analysis (single machine to infinite bus)

	ω	δ	ψ_{fd}	ψ_{1d}	ψ_{1q}	ψ_{2q}	v_1
R	0.07	3.43	1.14	0.46	0.08	0.19	0.33

4.1.3 Model Reduction

A 7^{th} order model is obtained without the PSS. There is no need for further reducing the order of original model since it contains only few number of states. Fig.4.2 illustrates the frequency response of the rotor speed of the generator rotor.

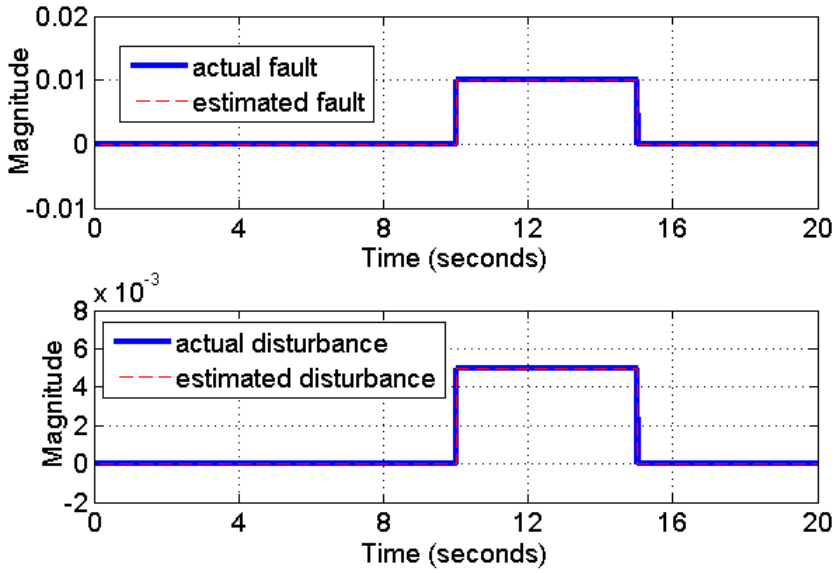

Figure 4.3: Actual and estimated signals for fault and disturbance (Single machine to infinite bus)

4.1.4 First Stage : System Identification

In this section, power system operation is influenced by one fault and one disturbance. Sudden changes in power system operation occur sometimes due to a single-phase or three phase faults in addition to load variations in the form of disturbances. A step change of 0.01 p.u amplitude is considered as a fault which affects the governor reference power. Meanwhile, a disturbance of 0.005 p.u amplitude is assumed to affect the exciter voltage reference. Both fault disturbance occur at the same time and last for 5 seconds. Fig.4.3 shows the estimated fault and disturbance signals against the true fault and disturbance signals. The fault and disturbance is successfully estimated by the designed UIO filter. As a result, the original system can be separated into three variations; 1) a fault and disturbance-free, 2) a fault-dependent, and 3) a disturbance-dependent. The fault-dependent subsystem reflects a power system operation which is disturbed by the occurrence of the fault. The governor reference power senses this fault and initiates a control signal to overcome its impact on power system operation. This definition is also applicable to disturbance-dependent subsystem, where the exciter voltage reference senses the presence of disturbance and initiates a control signal to overcome its impact. The only difference between fault and disturbance is the magnitude. Disturbance may refer to small-signal variations while fault reflects large-signal ones. Fig.4.4 shows the angular speed deviation profile in the presence of the fault and disturbance described above. The input control signal is assumed to act through

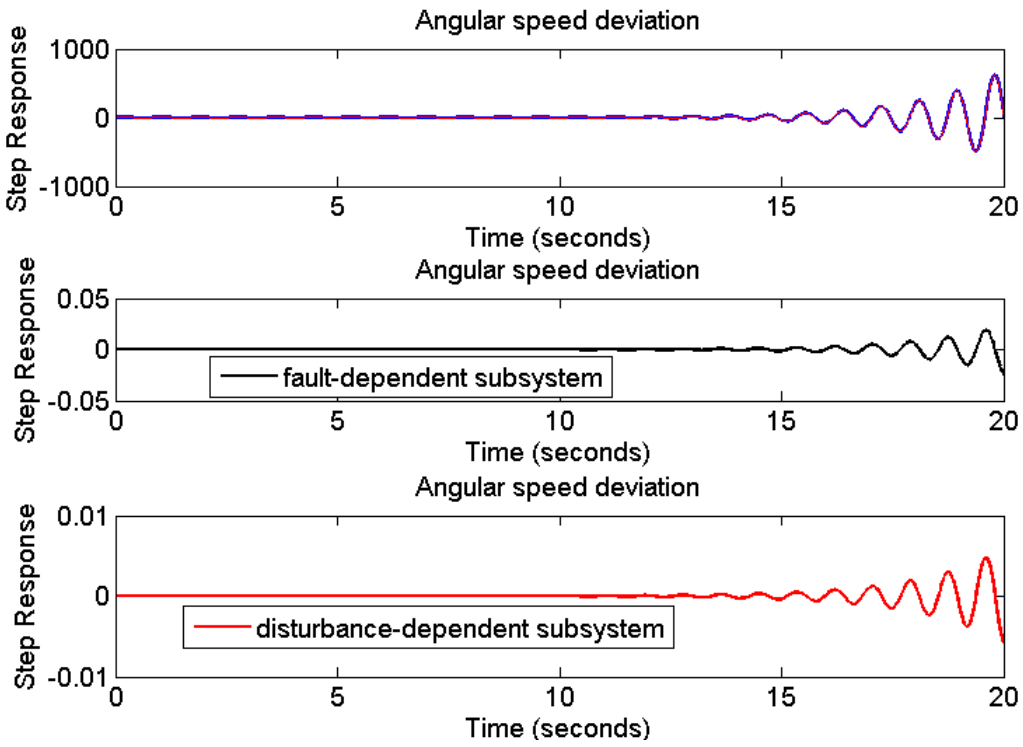

Figure 4.4: Original system profile against separated subsystems (Single machine to infinite bus)

the mechanical torque of the generator. A 1 p.u amplitude step signal is considered. In addition, this profile is compared with that associated with disturbance and fault-free subsystem. Both profiles exhibit unstable oscillatory behavior due to the unstable local mode eigenvalue observed when finding the eigenvalues of the linear model.

4.1.5 Second Stage : Robust Control Design

In the previous section, an UIO filter is designed for system decoupling and fault and disturbance estimation. A robust control design will be applied to each of the separated subsystems. The control input signal is the exciter voltage. The control signal will be fed back to the system through the mechanical torque matrix to achieve better damping and command tracking. A mixed H_∞ robust synthesis without pole placement is formulated using the LMI approach. The achieved damping ratio for the local mode is found to meet the minimum requirement. As a result, no pole placement is applied.

The standard form of S/KS mixed-sensitivity minimization is used as sown in Fig.3.5. The command tracking error minimization and disturbance and fault rejection are tackled using this formulation. As a result, three separate stabilizing controllers are designed for each subsystem.

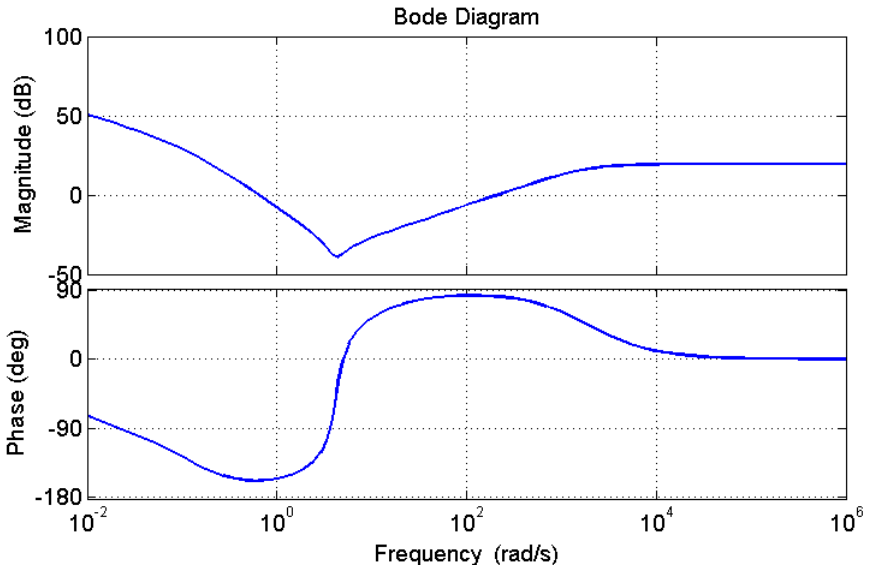

Figure 4.5: Frequency response of the weighting filter W_1 (Single machine to infinite bus)

The matlab library *magshape* in the Robust Control Toolbox [57] is used to design the weighting filters $W_1(s)$ and $W_2(s)$. For reference tracking problem, the following $W_1(s)$ and $W_2(s)$ were found to meet satisfactory the control design objectives. They are:

$$W_1(s) = \frac{9.36s^3 + 59.48s^2 + 235.7s + 814.5}{s^3 + 1951s^2 + 226.3s + 0.8653}, \quad W_2(s) = 1$$

The frequency response of $W_1(s)$ is shown in Fig.4.5. $W_1(s)$ has high values at low frequency to force the sensitivity function $S_o(s)$, which maps the command signal to the error one, to be small. Accordingly, zero steady state error could be obtained. Similarly, H_∞ mixed-sensitivity is applied to the fault and disturbance-dependent subsystems to suppress their impact on the system operation. The exogenous signal $w = r$ is replaced in Fig.3.5 by $w = f, d$ for fault and disturbance rejection. The following transfer functions W_1 and W_2 are found to reject the disturbance and fault:

$$W_1(s) = \frac{8.888s^2 + 11.58s + 1.293}{s^2 + 312s + 1164}, \quad W_2(s) = \frac{1.066}{s + 0.001}$$

A stabilizing controller for each subsystem is designed using the *hinfmix* command available in the LMI Control Toolbox [57]. The solved LMIs in matlab show that the guaranteed closed-loop H_∞ norm of fault and disturbance free, fault-dependent and disturbance-dependent variations are 9.3600, 0.000177 and 0.000175, respectively. The achieved H_∞ norm of both disturbance-

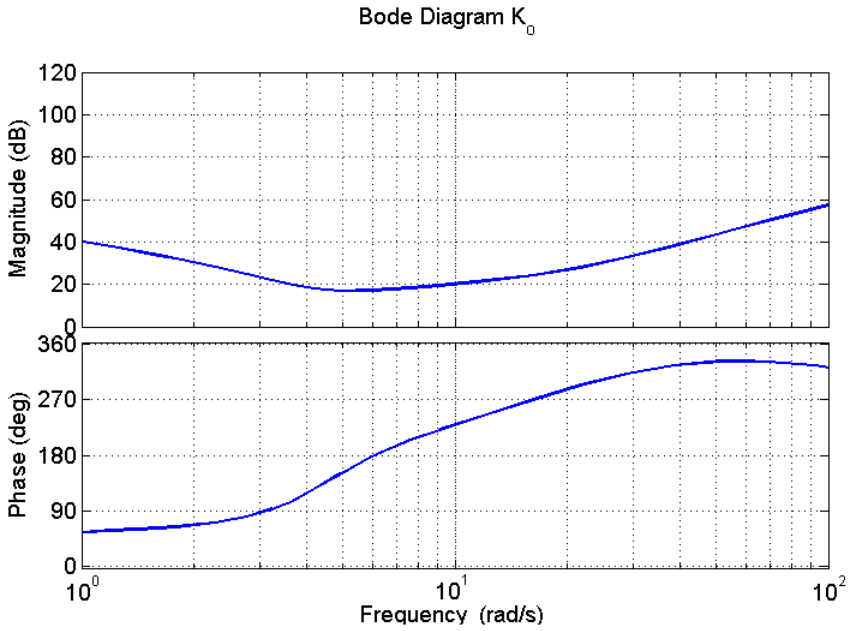

Figure 4.6: Designed controller for disturbance and fault-free subsystem (Single machine to infinite bus)

dependent and fault-dependent subsystems show the ability of the proposed architecture to suppress the effects of fault and disturbance. The designed controllers have an order equals to the sum of the order of open-loop model and weighting functions. Thus, 10^{th}-order controller for the three subsystems are obtained. The frequency response of the designed controllers are shown in Fig.4.6, Fig.4.7 and Fig.4.8.

The matlab function *slft* is utilized to form the closed loop system using the designed controllers as in Fig.3.6. Two-stage is the name of controller obtained using system identification and separation. This controller achieved a damping ratio of 0.2119. A comparison between the performance of centralized and two-stage controller is shown in Fig.4.9. Centralized controller (without two-stage) refers to that obtained when command, disturbance and fault signals (r, d and f) affect power system operation, simultaneously. In other words, the exogenous input w for centralized controller is a combination of three signals; r, d and f, respectively. It is worth mentioning that this approach is taken by B. Pal [15] and is recommended by G. Rogers [9]. For the two-stage controller, the exogenous input w contains only the command signal (r).

The following assumptions are considered for closed loop simulations:

1. *Command tracking*: A unit step signal is used for reference tracking objective.

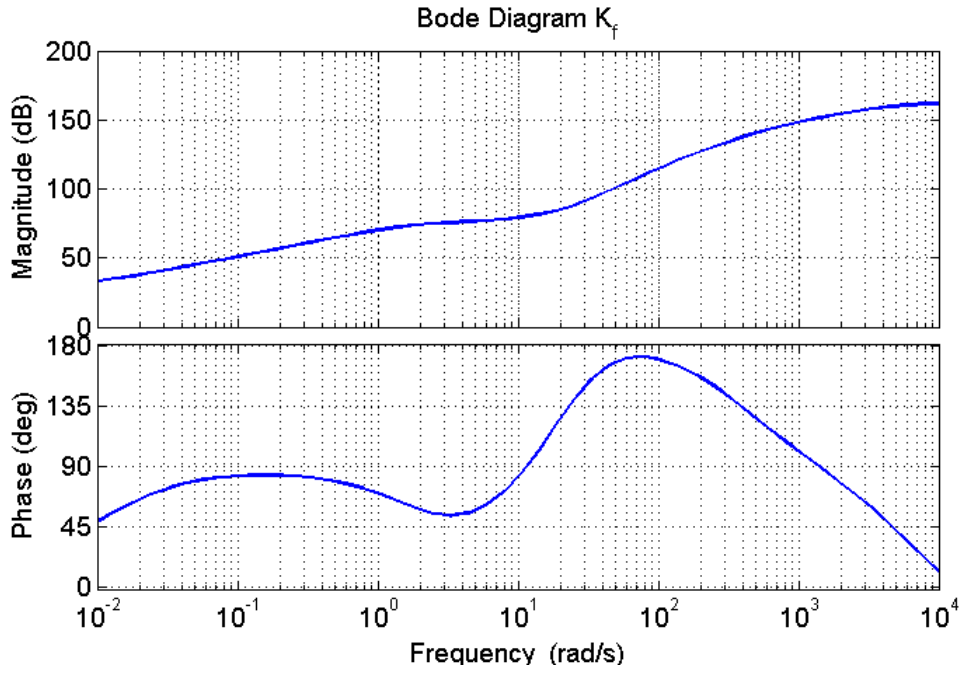

Figure 4.7: Designed controller for fault-dependent system (Single machine to infinite bus)

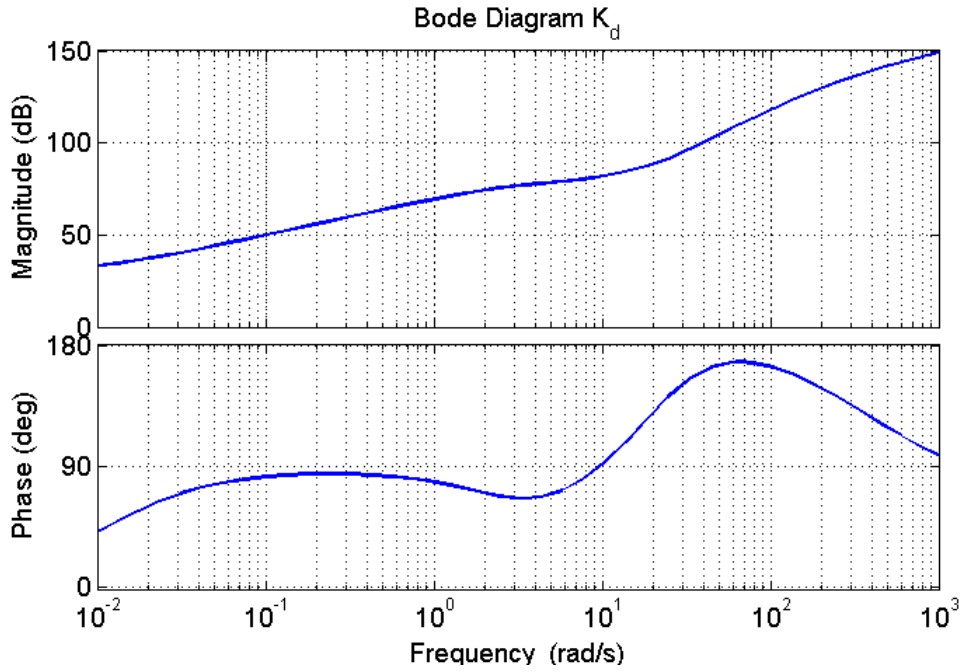

Figure 4.8: Designed controller for disturbance-dependent system (Single machine to infinite bus)

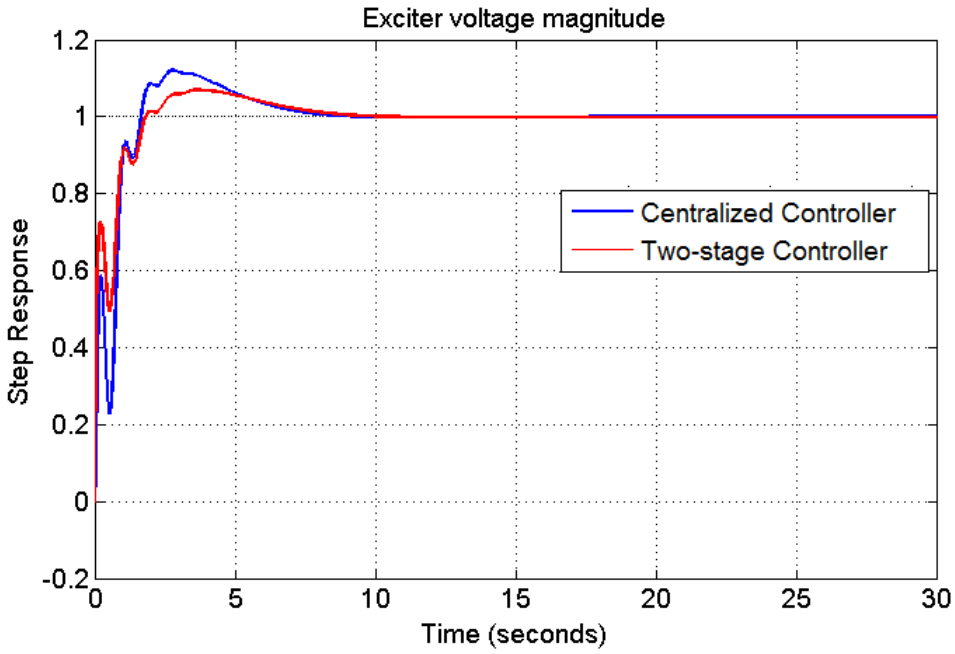

Figure 4.9: Performance of centralized and two-stage controllers (Single machine to infinite bus)

2. *Disturbance rejection*: A step signal of 0.005 per unit amplitude is assumed to affect the exciter reference voltage of generator 1. The disturbance occurs at time $t = 0$ and lasts for 30 seconds.

3. *Fault suppression*: A step signal of 0.01 amplitude is assumed to affect the turbine governor reference power of generator 1. The fault occurs at $t = 0$ and lasts also for 30 seconds.

Better damping for the local mode is achieved by the closed loop system for disturbance and fault-free subsystem. This can be seen from Fig.4.9, where the overshoot exhibited by two-stage and centralized controller is 1.07, 1.12; respectively. The overshoot is reduced by 41.98% in comparison with that exhibited by centralized controller. As a result, the impact of high overshoots on power exchange over transmission lines will be reduced. Accordingly, applying the UIO filter has a considerable impact on overshoot minimization and thus improving the overall power exchange over quite heavily transmission lines. Two-stage and centralized controllers almost achieve the same steady state time.

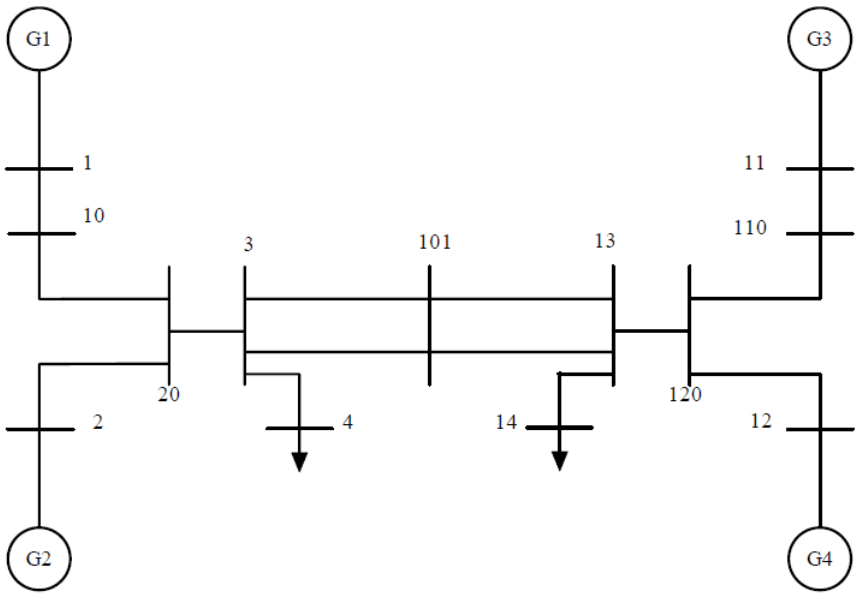

Figure 4.10: Single line diagram - Two Area System [9]

4.2 Two-area Four-machine System

The two-area four-machine system was developed to study the different modes of oscillations which could be observed in large and small power systems. [58]. Appendix *B* contains a detailed model descriptions of the system. Fig.B.1 shows the two-area four machine system. The two areas interconnected by weak tie-lines. Each area has two generators and a load. All synchronous machines are modeled with a slow excitation system (IEEE-DC1A) and a governor system. The power transfer over the tie lines from area 1 to area 2 is 400 MW. As a result, the system is quite heavily stressed. The active load is modeled as 50% constant current and 50% constant impedance; the reactive load is modeled as constant impedance.

4.2.1 Full-order Model and Small Signal Analysis

A sub-transient model with four equivalent coils on the rotor is used to represent all the generators. An equivalent damper coil is modeled in the direct-axis besides the field coil. In addition, there is two coils in the quadrature-axis. The generators are equipped with slow excitation system (IEEE-DC1A). Accordingly, each generator has 13 states. There is also one state related with the installation of Static VAr Compensator (SVC). Active and reactive load modulations are also considered which adds 5 more states to the complete nonlinear model. As a result, a $586th$-order nonlinear model is obtained. A power transfer between the two areas of 400 MW was chosen to represent the nominal plant. This operating point was also used to linearize the

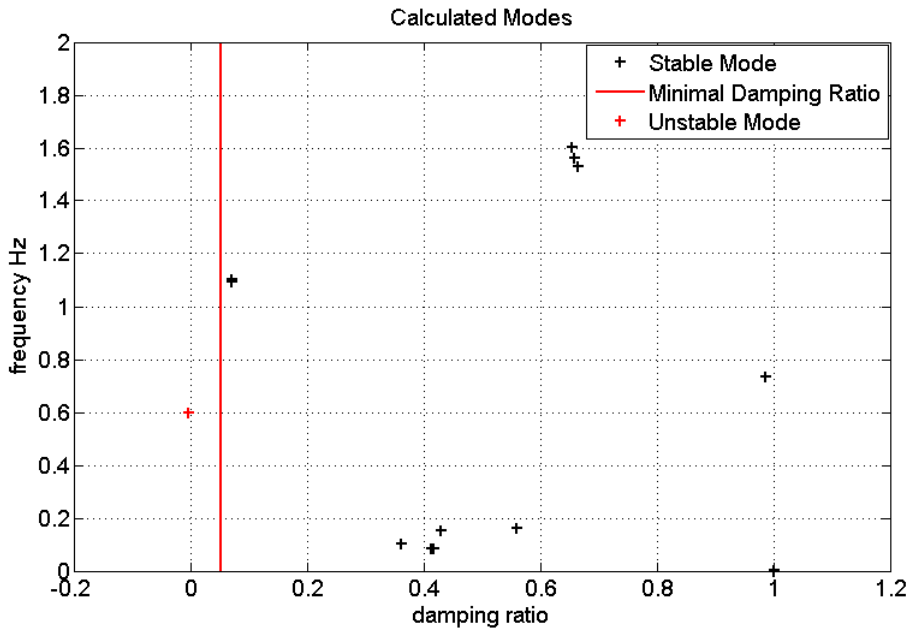

Figure 4.11: Two-area four machines - small signal analysis

Table 4.3: Residual analysis (two-area system)

	ω_1	ω_2	ω_3	ω_4	δ_1	θ_{13}	I_3	P_2	V_3	V_{101}
SVC_3	0.003	0.002	0.006	0.005	0.217	0.388	0.868	0.824	0.117	0.141
SVC_{101}	0	0	0.001	0.001	0.036	0.108	0.058	0.314	0.023	0.028
SVC_{13}	0.003	0.002	0.011	0.01	0.142	0.905	1.659	1.179	0.205	0.254

nonlinear model. The choice of this point reflects a stressed power system operation where the presence of inter-area modes plays a crucial role in determining the tie-lines transmission capacity. The eigenvalue analysis shows the presence of poorly damped unstable inter-area mode $0.016 \pm j3.764$ with frequency 0.599 Hz and damping ratio 0.004. An acceptable damping is to be achieved after applying the two-stage robust control. Fig. 4.11 shows the eigenvalues of the system.

4.2.2 Selection of Measurements and Control Site Locations

Residual analysis is used to study the strength of stabilizing control signals and to evaluate the controllers performance at different places for this inter-area mode. The candidate input signals to SVC are bus voltage magnitude, generator rotor speeds and injected current from certain bus. Table 4.3 shows the residue related with different SVC locations and possible input signals.

The rows correspond to SVC located at bus 3, 101 and 13 and the columns correspond to measurements. ω_i denotes the rotor speed of generator i. θ_{12} refers to the voltage angle difference between bus 1 and 2. V_3 and I_3 refer to the voltage at and current injected from bus 3.

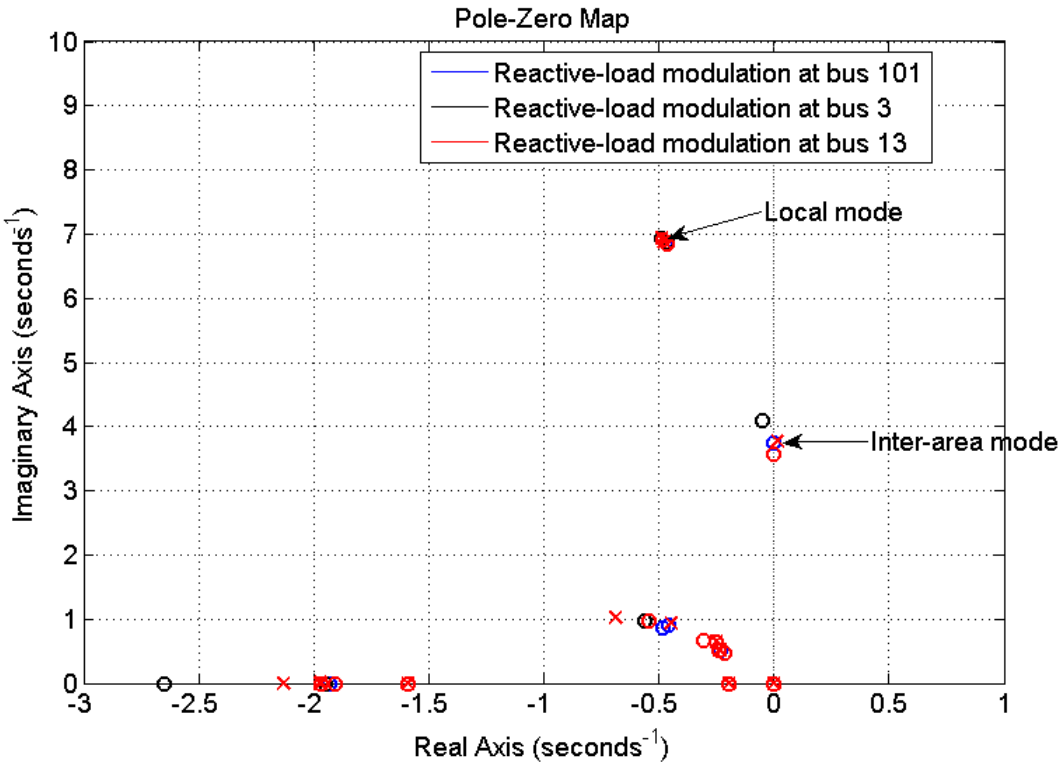

Figure 4.12: Dominant poles and zeros due to reactive load modulation (Two-area system)

Fig.4.12 shows the dominant poles and zeros due to reactive load modulation at bus 3, 12 and 101, respectively. From the calculation results shown in Table 4.3 and Fig.4.12, the following conclusions can be outlined:

1. I_3 and P_2 are the most efficient stabilizing signals because they have high residues.

2. Fig.4.12 shows that in all cases, zeros effectively cancel the local modes and the governor modes. With reactive modulation at bus 13 and bus 101, zeros are very close to the inter-area mode. As a result, A SVC at bus 13 and bus 101 is not suitable for damping the inter-area mode. With modulation at bus 3, the grid still has a zero close to the inter-area mode. However, the zero is at a higher frequency than the pole in comparison with the other two scenarios. The closeness of zeros to inter-area modes limit the amount of damping that can be achieved. In physical terms, placing SVC at bus 3 for voltage control will add synchronizing torque to the inter-area mode. Accordingly, the SVC will be sited at bus 3. Current magnitude injected from bus 3 will be used for damping control design. The analysis presented in the literature identified the best location at bus 101, further investigation should be conducted to justify the conclusion of this work.

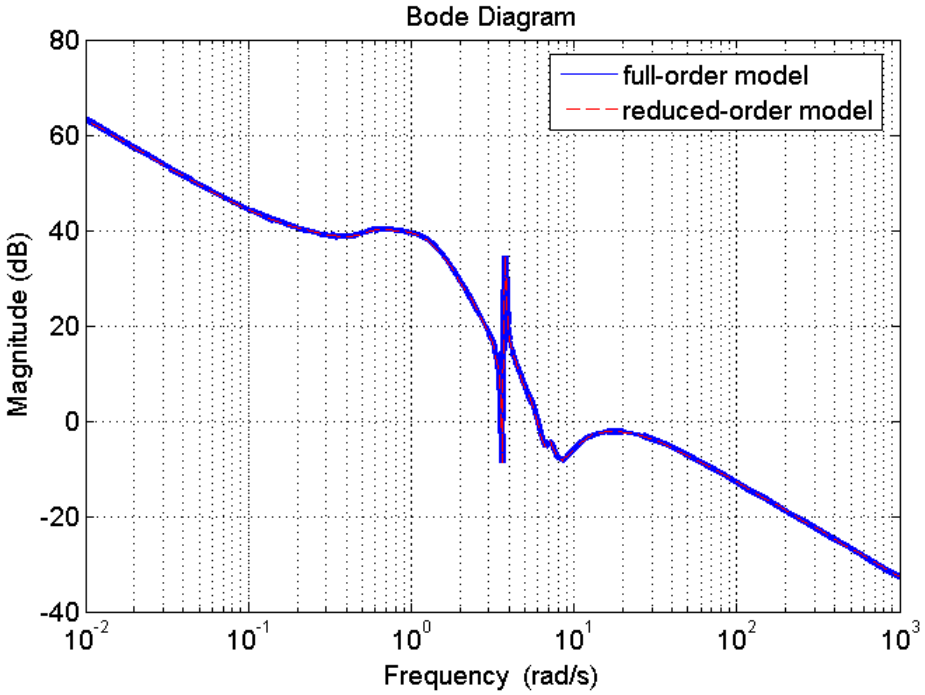

Figure 4.13: Frequency response of full and reduced-order model (Two-area system)

4.2.3 Model Reduction

A 58^{th}-order model was obtained in the previous sections. The solution in LMI framework is based on iterative-γ methods and thus needs a large amount of time for calculation. Meanwhile, not all states of a power system are dominant. In fact, the characteristics of this small system can be contained by no more than a few states. Therefore, the original order model is reduced to a 16^{th}-order model using optimal hankel norm approximation. Fig.4.13 shows the frequency responses of the full and reduced-order model. Conclusion 2, mentioned above, is observed once a gain in the bode plot. Placing a SVC at bus 3 adds a zero close to the inter-area mode. This can be seen from the two peaks in the bode plot at almost the same frequency.

4.2.4 First Stage : System Identification

One fault and one disturbance are assumed to affect the power system operation. The fault affect the grid through the turbine governor reference power of generator 1. The fault could represent a three-phase fault at a certain bus. In addition, the disturbance affects the grid through the exciter voltage reference of generator 1. Faults and disturbances are included in power system model through the matrices B_f and B_d as shown in 3.10. In this section, an example is given to illustrate the usability of power system identification and separation proposed in previous sections.

The fault is represented by a step change in the load of 0.01 pu and lasts for 5 seconds. In addition, the disturbance is represented by a step change of 0.005 pu and lasts also for 5 seconds. Both fault and disturbance are assumed to occur at the same time. The UIO observer design is initiated by checking the rank requirements of the power system state space model 3.10 and 3.11. Fig.4.14 shows the actual and estimated signals for fault and disturbance.

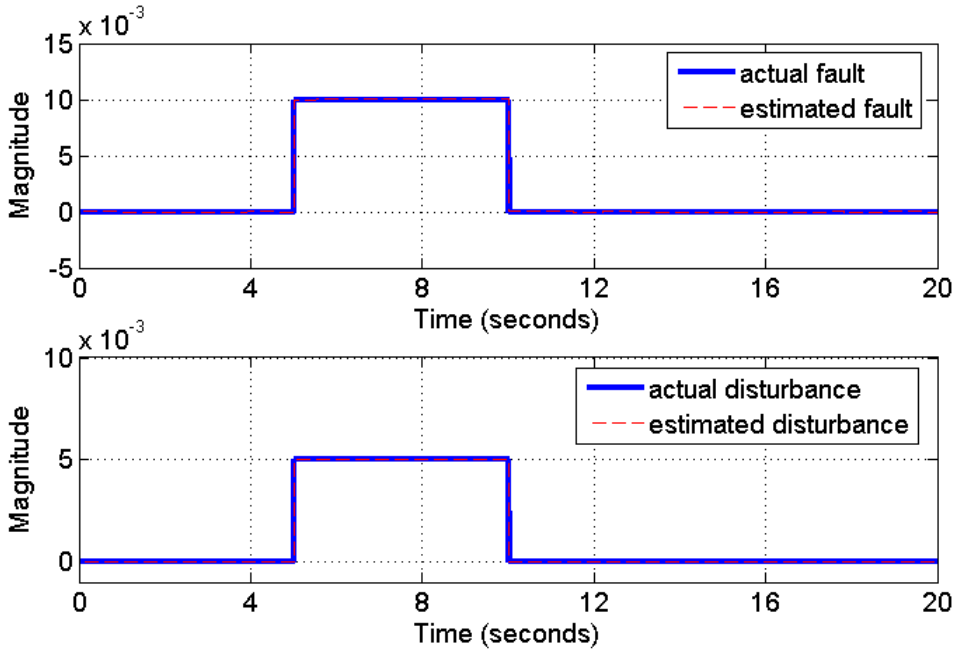

Figure 4.14: Actual and estimated signals for fault (Two-area system)

The designed UIO successfully estimated the fault and disturbance, this enables us to separate the original system into three variations; 1) a fault and disturbance-free, 2) a fault-dependent, and 3) an actuator fault-dependent. A separate robust control design will be applied to each subsystem in the next stage. Fig.4.15 shows voltage deviation profile at bus 3 in the presence of the fault and disturbance which are described above. The input signal to the SVC is a step signal of 1 pu. In addition, this profile is compared with that associated with disturbance and fault-free subsystem. Both profiles exhibit growing oscillatory behavior due to the poorly inter-area mode. Fig.4.15 shows also the voltage deviation profiles associated with fault-dependent and disturbance-dependent subsystems. An oscillatory behavior is also observed in both subsystems.

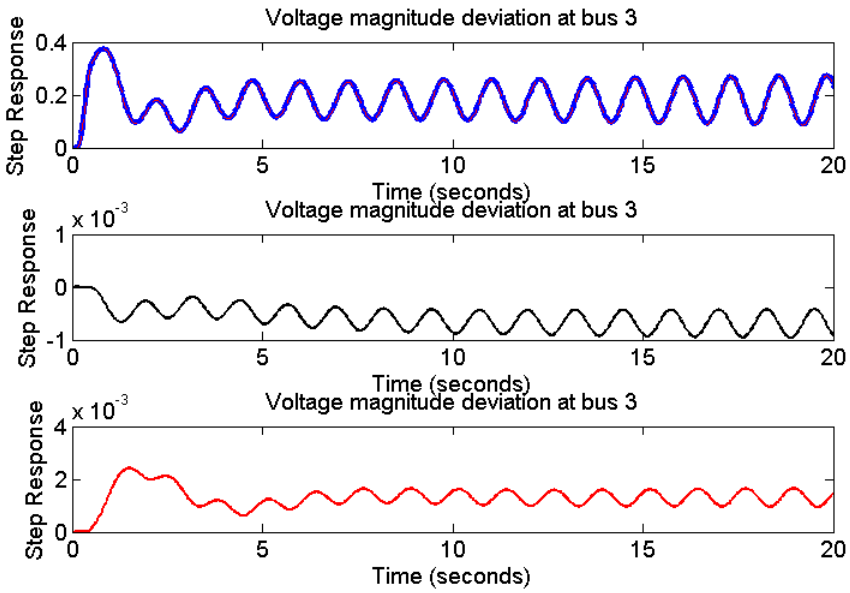

Figure 4.15: Original system profile against separated subsystems (Two-area system)

4.2.5 Second Stage: Robust Control Design

We are now ready to design our robust SISO controller for the three subsystems. The control input signal is the injected current from bus 3 where SVC is sited as illustrated previously. For the fault and disturbance-free variation, a mixed H_∞ robust synthesis with pole placement is formulated using the LMI approach. As a result, the closed-loop poles may be allocated in a prescribed region. In this research, the LMI region is chosen to be a conic sector with apex at the origin and inner angle θ such that the minimum required damping ratio $\zeta_{min} = \cos^{-1}\frac{\theta}{2}$ is achieved. The design requirements in power systems is to ensure that the oscillations settle within 10-15 s [57]. This can be obtained if the poles of closed loop system are placed within a conic sector of inner angle 174.27 degree with an apex at the origin which ensures a minimum damping ratio of 0.05.

Fig.3.5 shows the S/KS mixed-sensitivity minimization in standard form. This form is used in this research to minimize the reference tracking error. In addition, the standard form is also used to suppress the impact of faults and disturbances. Accordingly, three separate stabilizing controllers are designed for each subsystem. The weighting functions $W_1(s)$ and $W_2(s)$ are designed via the *magshape* library in the Robust Control Toolbox in matlab [7]. As illustrated in chapter 3, there are no explicit rules for designing the weighting functions. As a result, several designs are tested against the stability and performance specifications. For reference tracking

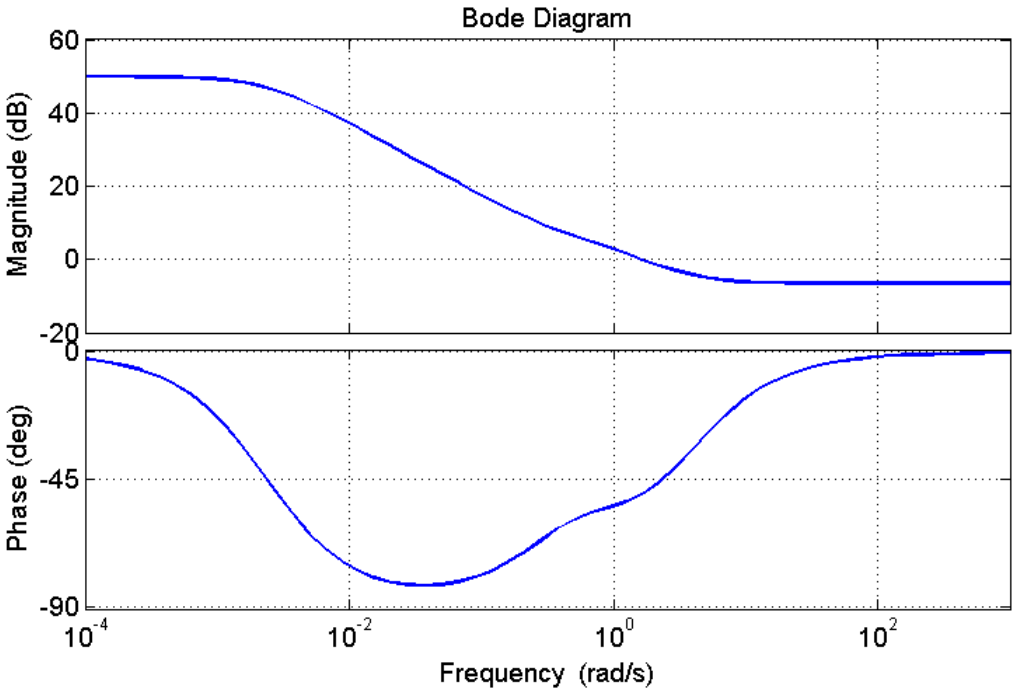

Figure 4.16: Frequency response of the weighting filter W_1 (Two-area system)

problem, the following $W_1(s)$ is found to satisfactory meet the control design objectives.

$$W_1(s) = \frac{0.4697s^2 + 1.797s + 0.6093}{s^2 + 0.8368s + 0.001949}, \quad W_2(s) = 1$$

Fig.4.16 shows the frequency response of W_1 which exhibits a low pass filter for reference tracking error rejection. At frequencies below $0.01 rad/s$, the low pass filter has approximately a value of 50 dB. According to equation (3.61) in previous sections, this high value guarantees that the sensitivity transfer matrix which maps the command signal to the error one is very small. As a result, zero steady state error is ensured. Similarly, H_∞ mixed-sensitivity is applied to the fault and disturbance-dependent subsystems to suppress their impact on the system operation. The standard form of mixed-sensitivity minimization is also applied as in Fig. 3.5 by replacing the reference signal $w = r$ with $w = f, d$. For fault and disturbance rejection, the following transfer function W_1 is found to satisfactory reject the disturbance and fault.

$$W_1 = \frac{0.003085s^2 + 0.1409s + 0.1983}{s^2 + 425.7s + 608.1}, \quad W_2(s) = \frac{1.066}{s + 0.001}$$

Fig.4.17 shows the frequency response of W_1 which exhibits a high pass filter for fault and disturbance rejection. The sensitivity transfer function S is needed to have low values in a certain

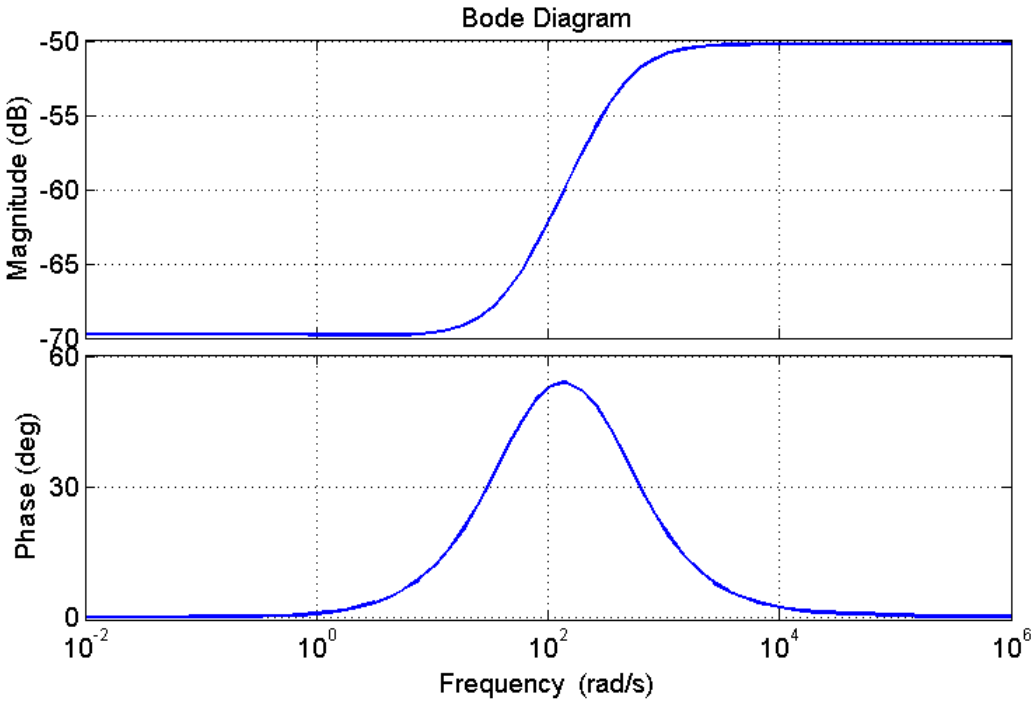

Figure 4.17: Frequency response of the weighting filter W_1 (Two-area system)

frequency range to restrain the effects of faults and disturbances on system operation.

The *hinfmix* command in the LMI Control toolbox [7] was utilized to solve for a stabilizing controller that satisfies the set of LMIs described in chapter 3. Pole placement is applied to ensure that minimum damping is achieved. The solved LMIs in matlab shows that the guaranteed closed-loop H_∞ norm of fault and disturbance-free, fault-dependent and disturbance-dependent variations are 1.3000, 0.0031 and 0.0006, respectively. The achieved H_∞ norm of both disturbance-dependent and fault-dependent subsystems show the ability of the proposed architecture to suppress the effects of fault and disturbance. The order of the designed controller by solving the LMIs is the sum of the order of open-loop model and weighting functions. Thus, $18^{th}, 19^{th}$ and 19^{th}-order controller for the three subsystems are obtained,respectively. Fig.4.18, Fig.4.19 and Fig.4.20 show the frequency response of the designed controller. The standard H_∞ formulation synthesizes controllers with the dynamics required to stabilize the grid and to achieve the performance objectives. As mentioned in previous sections, the designed controller has a state space representation such in equations (3.81)-(3.82). As a result, the dynamics of synthesized controller differs from that of the original system. The designed controllers for fault-dependent and disturbance-dependent subsystems contain a zero close to that of the inter-area oscillation. This issue affects the amount of damping which can be achieved by

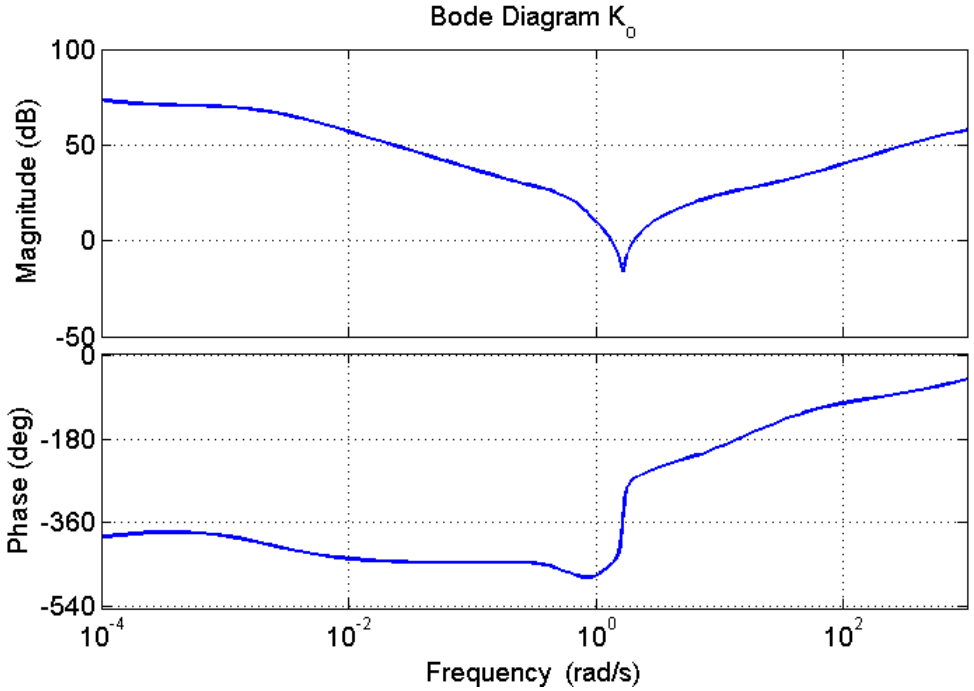

Figure 4.18: Designed controller for disturbance and fault-free subsystem (Two-area system)

the controller. In addition, non-minimum phase zeros affect the transient response of the closed-loop system along with the poles. These zeros determine the minimum bandwidth requirements weighting functions must have to achieve the stability and performance objectives [8].

The closed loop system as in Fig.3.6 is formed using the designed controller for each subsystem via the matlab function *slft*. Fig.4.21 shows a comparison between the performance of centralized and two-stage controller. Centralized and two-stage controllers differ in the number of signals contained in the exogenous signal w. The exogenous input to the centralized controller contains; command signal(r), disturbance signal (d) and fault signal (f). These signals are used to generate Fig.4.21. After applying a separation filter, the exogenous signal to the two-stage controller contains only the command signal (r). The two-stage controller achieves a damping ratio of 0.0604 while centralized controller achieved a damping ratio of 0.0584. The closed loop system is subjected to the following signals in the exogenous input w:

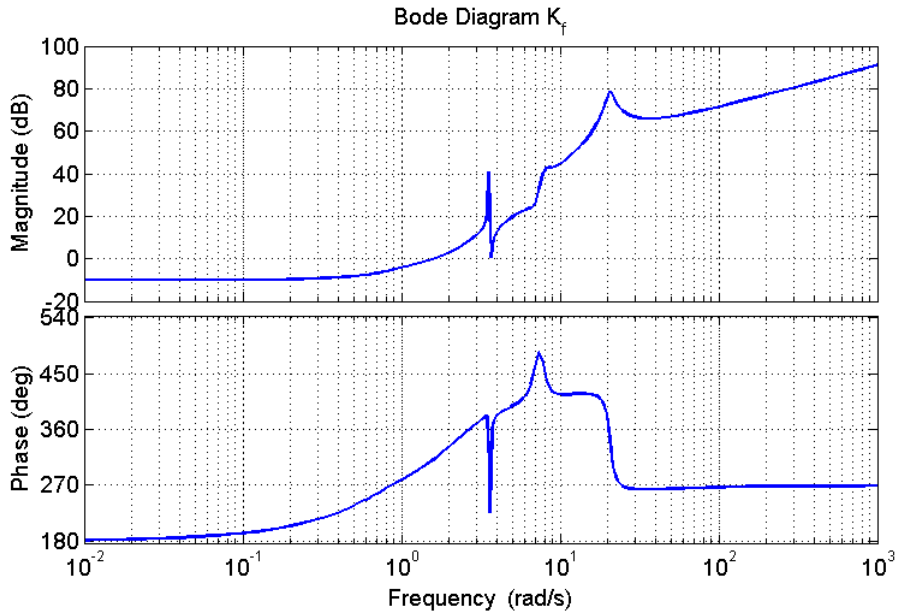

Figure 4.19: Designed controller for fault-dependent system (Two-area system)

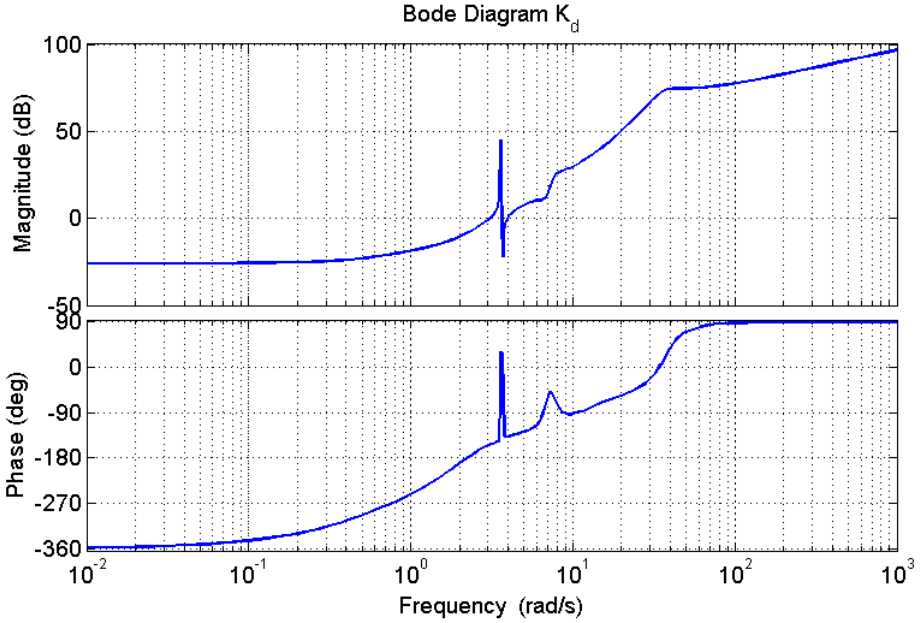

Figure 4.20: Designed controller for disturbance-dependent system (Two-area system)

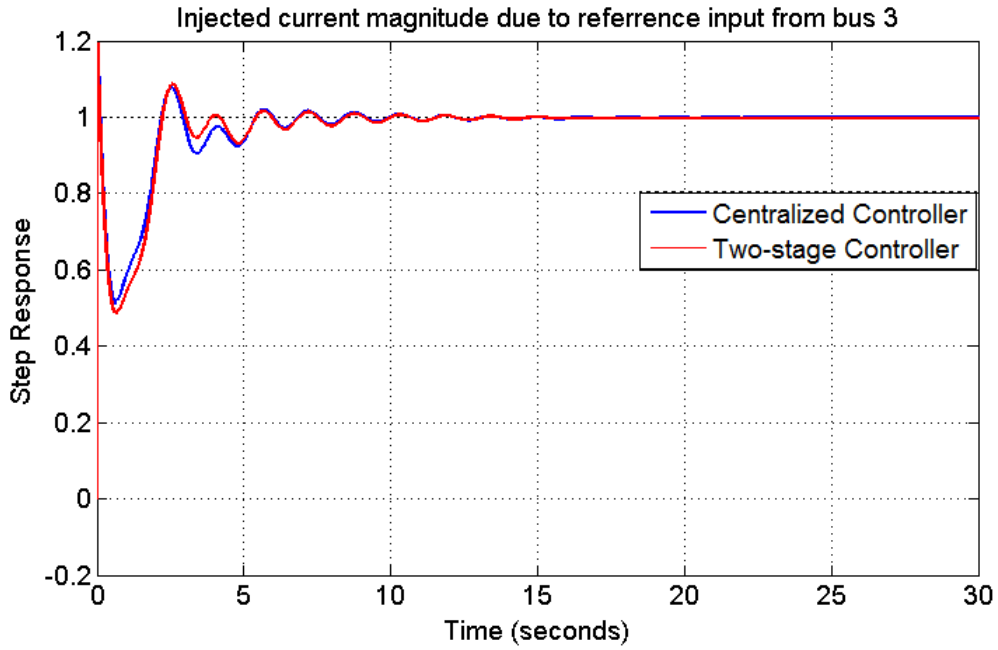

Figure 4.21: Performance of centralized and two-stage controllers with pole placement (Two-area system)

1. *Command tracking*: A unit step signal is used for reference tracking objective.

2. *Disturbance rejection*: A step signal of 0.005 per unit amplitude is assumed to affect the exciter reference voltage of generator 1. The disturbance occurs at time $t = 0$ and lasts for 30 seconds.

3. *Fault suppression*: A step signal of 0.01 amplitude is assumed to affect the turbine governor reference power of generator 1. The fault occurs at $t = 0$ and lasts also for 30 seconds.

The poles of the closed loop system are forced to lie within the prescribed region D specified before solving the LMIs. It can be noticed from Fig.4.21, that two-stage controller achieves slightly better damping in comparison with the centralized one. The two-stage controller achieved almost a 0.4% improvement in comparison with the damping ratio achieved using a standard H_∞ controller applied to the power system model without separation. This little improvement is caused by the application of pole placement which serves as a constraint forcing the closed loop poles to lie within certain limits regardless wither separation filter is used or not.

Fig.4.22 shows the closed loop performance of centralized and two-stage controllers without using pole placement. The achieved damping by two-stage controller in this case is 0.0201. It is noticed from the plot that the overshoot for two-stage and centralized controllers are 1.03 and 1.25, respectively. The overshoot is reduced by 17.60% due to the application of separation filter. In addition, the two-stage controller achieves shorter steady-state in comparison with the centralized controller. The simulation time was extended over 15 seconds to show the time needed to reach steady-state. However, the achieved damping ratio is still below the minimum requirements. As a result, pole placement must be used as described above to achieve acceptable damping.

In conclusion, the two-stage controller decreases the overshoot experienced at the beginning of the transient response. The performance of two-stage controller minimizes considerably the overshoot when pole placement isn't applied. If pole placement is required to achieve the minimum damping ratio, the improvement introduced by two-stage controller is lower. Overshoot minimization will reduce its impact of on power exchange over transmission lines, especially in quite heavily stressed grids. Fig.4.23 shows clearly the ability of two-stage controller to strain the impact of the fault and disturbance.

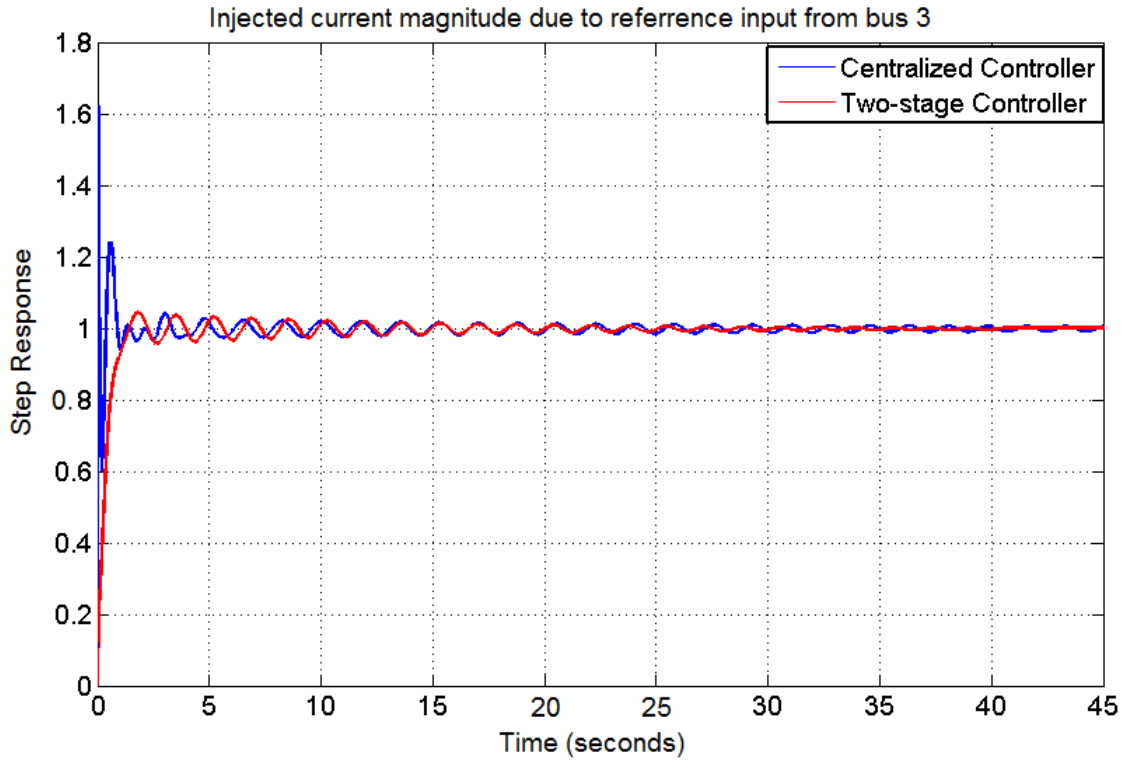

Figure 4.22: Performance of centralized and two-stage controllers without pole placement (Two-area system)

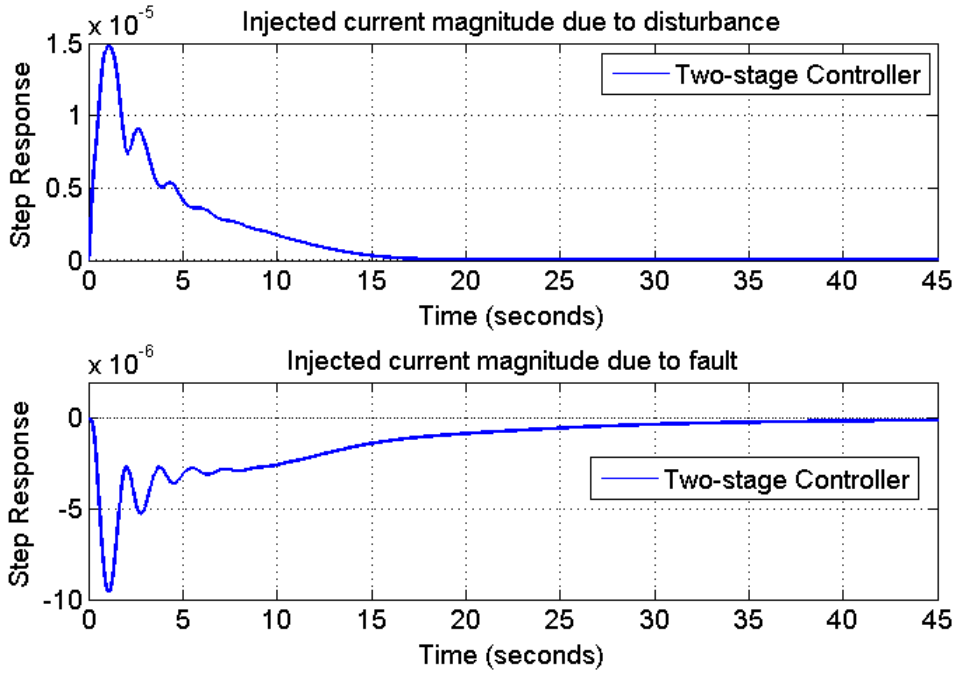

Figure 4.23: Closed loop system for disturbance and fault-dependent system (Two-area system)

5

CONCLUSIONS AND FUTURE WORK

5.1 Conclusions

In this thesis, the design procedure of a centralized two-stage robust control was described for low-frequency inter-area oscillations. Controllability/observability based residual analysis were used to study the strength of candidate control signals and to evaluate the controllers performance at different locations. The order of the controller synthesized by LMI approach is the same as the open-loop system order including the weighting functions. As a result, model reduction via the optimal hankel norm approximation was utilized to reduce power system order and to ease the control design. An unknown input observer (UIO) was used thereafter to separate the disturbances and faults from power system. Three subsystems were obtained from the system identification and separation stage. Each subsystem will be separately used for control design in the second stage. The robust SISO controller synthesis was formulated as a mixed-sensitivity H_∞ output-feedback control problem. A regional pole placement might be required to achieve the minimum damping. The LMI framework was used in the control design. The design method was tested on two study systems. Linear analysis demonstrated the robustness and efficiency of the designed controllers. The following conclusions can be drawn from the simulation results:

- Residual analysis were effective in studying the strength of candidate control signals of differing types.

- Active powers and current magnitudes were found to be good choices as control signals for damping inter-area modes.
- Optimal hankel norm approximation provided good model reduction to ease control design and avoided complexity in designed controllers .
- Unknown Input Observer (UIO) was found to provide almost complete estimation and separation for faults and disturbances. This lessens the complicated trade-offs design objectives inherent in robust control design like reference tracking,disturbance rejection and noise attenuation. Three subsystems were obtained by the UIO filter. A separate control design is applied to each subsystem.
- The proposed architecture considerably minimizes the overshoot when pole placement isn't applied. If pole placement is required to achieve the minimum damping ratio, the improvement introduced by two-stage controller is less. The architecture successfully suppress the impact of disturbances and faults on the operation of the system.

5.2 Future Work

This research achieved promising results in applying two-stage robust control for damping low-frequency inter-area oscillations. This research establishes the basis for further development in the field of small signal stability of power systems. In addition, the work serves as basic understanding for the state-of-art technologies used in damping oscillations in power systems such as FACTS devices.

The two-stage robust control architecture proposed in this research is based on centralized approach. Remote measurements are collected based on good observability of the inter-area modes. Control signals are sent by the centralized controllers to several control devices simultaneously. Several disadvantages are associated with this approach. For example, time-delays are increased by centralized controllers caused by collecting measurements to control center and re-routing them or control signals to control sites. This could result in increased investments for communication network and central computers, and interactions between control loops. A decentralized approach in contrast has less time-delays, less investment for hardware, and reduced interactions between control loops. To address the above limitations, the proposed two-stage robust control can be evolved into a decentralized architecture in the future. Evaluation of its

usability in damping low-frequency inter-area oscillations will also be done.

6

Appendix A

Single machine to infinite bus system parameters

Fig. A.1 shows the system representation applicable to a thermal generating station consisting of four 555 MVA, 24 kV, 60 Hz units [2].

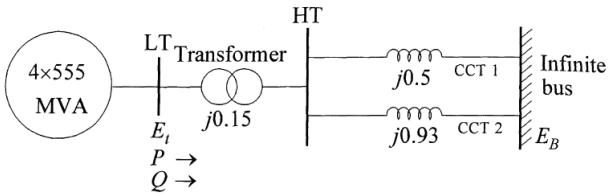

Figure A.1: Single machine to infinite bus test system [2]

The network reactances shown in the figure are in per unit on 2220 MVA, 24 kV base (referred to the LT side of the step-up transformer). Resistances are assumed to be negligible [2]. The system condition in per unit on the previously mentioned base units is as follows [2]:

$P = 0.9$, $Q = 0.3$ (overexcited), $E_t = 1.0\underline{/36^\circ}$, $E_B = 0.995\underline{/0^\circ}$

The generators are to be modeled as a single equivalent generator represented by detailed model with the following parameters expressed in per unit on 2220 MVA, 24 kV base [2]:

$X_d = 1.81$, $X_q = 1.76$, $X'_d = 0.3$, $X'_q = 0.65$, $X_l = 0.16$

$X''_d = 0.23$, $X''_q = 0.25$, $R_a = 0.003$, $H = 3.5$, $K_D = 0$

$T'_{d0} = 8.0$ s, $T'_{q0} = 1.0$ s, $T''_{d0} = 0.03$ s, $T''_{q0} = 0.07$ s

7

Appendix B

Two-area four-machine system parameters

A weak tie line connects the two similar areas connected. There are two coupled generation units in each area, each having a rating of 900 MVA and 20 kV. The generator parameters in per unit on the rated MVA and kV base are as follows [45]

X_d = 1.8

V_q = 1.7

$\dot{X}_d$ = 0.3

$\dot{X}_q$ = 0.55

R_a = 0.0025

$\dot{T}_d$ = 8.0 s

$\dot{T}_q$ = 0.4 s

H_1, H_2 = 6.5

H_3, H_4 = 6.175

K_D = 0

Each step-up transformer has an impedance of $0 + j0.15$ per unit on 900 MVA and 20/30 kV base [59], and has an off-nominal ratio if 1.0 [59]. The transmission system nominal voltage is 230 kV [59]. The line lengths are identified in Fig. B.1. The parameters of the lines in per unit on 100 MVA, 230 kV base are [59].

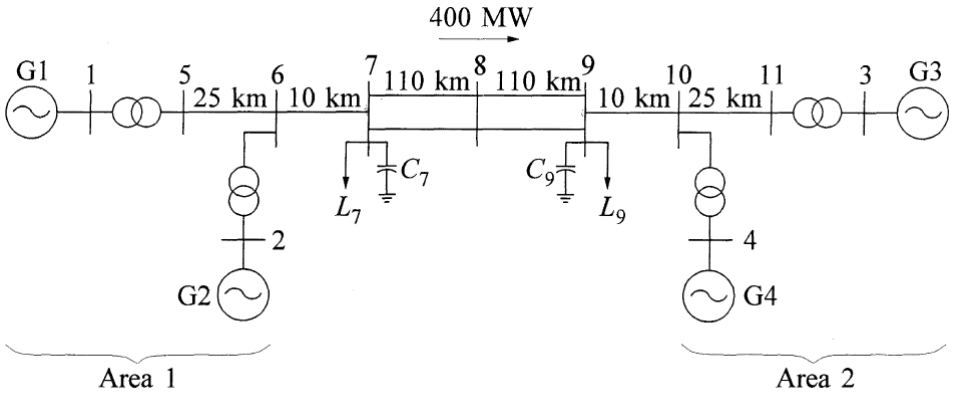

Figure B.1: Two-area four-machine test system [2]

R = 0.0001 pu/km

X_l = 0.001 pu/km

B_c = 0.00175 pu/km

The system is operating with area 1 exporting 400 MW to area 2, and the generating units are loaded as follows [2]:

G1 : $P = 700MW, Q = 185MVAr, E_t = 1.03\underline{/20.2^\circ}$

G2 : $P = 700MW, Q = 235MVAr, E_t = 1.01\underline{/10.5^\circ}$

G3 : $P = 719MW, Q = 176MVAr, E_t = 1.03\underline{/-6.8^\circ}$

G4 : $P = 700MW, Q = 202MVAr, E_t = 1.01\underline{/-17.0^\circ}$

The loads and reactive power supplied (Q_c) by the shunt capacitors at buses 7 and 9 area as follows [2]:

Bus 7 : $P_l = 976MW, Q_l = 100MVAr, Q_c = 200MVAr$

Bus 9 : $P_l = 1767MW, Q_l = 100MVAr, Q_c = 350MVAr$

The self-excited dc exciter parameters are as follows:

K_A = 20.0

T_A = 0.055

T_E = 0.36

K_F = 0.125

T_F = 1.8

A_{ex} = 0.0056

B_{ex} = 1.075

T_R = 0.05

Bibliography

[1] P. W. Sauer and M. Pai, *Power system dynamics and stability*, vol. 4. Prentice Hall Upper Saddle River, NJ, 1998.

[2] P. Kundur, N. J. Balu, and M. G. Lauby, *Power system stability and control*, vol. 7. McGraw-hill New York, 1994.

[3] Y. Zhang and A. Bose, "Design of wide-area damping controllers for interarea oscillations," *Power Systems, IEEE Transactions on*, vol. 23, no. 3, pp. 1136–1143, 2008.

[4] B. Pal and B. Chaudhuri, *Robust control in power systems*. Springer Science & Business Media, 2006.

[5] K. Zhou, J. C. Doyle, K. Glover, *et al.*, *Robust and optimal control*, vol. 40. Prentice hall New Jersey, 1996.

[6] G. J. Balas, *Mu-Analysis and Synthesis Toolbox for Use with MATLAB®: User's Guide*. MathWorks, Incorporated, 1998.

[7] P. Gahinet, A. Nemirovskii, A. J. Laub, and M. Chilali, "The lmi control toolbox user's guide," 1995.

[8] S. Skogestad and I. Postlethwaite, *Multivariable feedback control: analysis and design*, vol. 2. Wiley New York, 2007.

[9] G. Rogers, "Power system oscillations," *Massachusetts: Kluwer Academic Publishers*, 2000.

[10] E. Larsen and J. Chow, "Svc control design concepts for system dynamic performance," *Application of Static Var Systems for System Dynamic Performance*, pp. 36–53, 1987.

[11] I. Kamwa and L. Gerin-Lajoie, "State-space system identification-toward mimo models for modal analysis and optimization of bulk power systems," *Power Systems, IEEE Transactions on*, vol. 15, no. 1, pp. 326–335, 2000.

[12] C. W. Taylor, D. C. Erickson, K. E. Martin, R. E. Wilson, and V. Venkatasubramanian, "Wacs-wide-area stability and voltage control system: R&d and online demonstration," *Proceedings of the IEEE*, vol. 93, no. 5, pp. 892–906, 2005.

[13] N. Martins, A. Barbosa, J. Ferraz, M. Dos Santos, A. Bergamo, C. Yung, V. Oliveira, and N. Macedo, "Retuning stabilizers for the north-south brazilian interconnection," in *Panel session on system reliability as affected by power system stabilizers, 1999 IEEE PES Summer Meeting, Edmonton, Canada*, 1999.

[14] H. Breulmann, E. Grebe, M. Lösing, *et al.*, "Analysis and damping of inter-area oscillations in the ucte/centrel power system," 2000.

[15] B. Pal, A. Coonick, and B. Cory, "Robust damping of inter-area oscillations in power systems with superconducting magnetic energy storage devices," in *Generation, Transmission and Distribution, IEE Proceedings-*, vol. 146, pp. 633–639, IET, 1999.

[16] A. Al-Ebrahim, N. Al-Shahrani, and M. Al-Shaikh, "Gcc interconnection grid: Operational studies for the gcc interconnection with united arab emirates (uae)," 2012.

[17] F. Schleif and J. White, "Damping for the northwest-southwest tieline oscillations-an analog study," *Power Apparatus and Systems, IEEE Transactions on*, no. 12, pp. 1239–1247, 1966.

[18] F. Schleif, G. Martin, and R. R. Angell, "Damping of system oscillations with a hydrogenerating unit," *Power Apparatus and Systems, IEEE Transactions on*, no. 4, pp. 438–442, 1967.

[19] C. Concordia, "Performance of interconnected systems following disturbances," *Spectrum, IEEE*, vol. 2, no. 6, pp. 68–80, 1965.

[20] M. Klein, G. Rogers, P. Kundur, *et al.*, "A fundamental study of inter-area oscillations in power systems," *IEEE Transactions on Power Systems*, vol. 6, no. 3, pp. 914–921, 1991.

[21] H. Ellis, J. Hardy, A. Blythe, and J. Skooglund, "Dynamic stability of the peace river transmission system," *Power Apparatus and Systems, IEEE Transactions on*, no. 6, pp. 586–600, 1966.

[22] F. R. Schleif, H. D. Hunkins, G. E. Martin, and E. E. Hattan, "Excitation control to improve powerline stability," *Power Apparatus and Systems, IEEE Transactions on*, no. 6, pp. 1426–1434, 1968.

[23] E. Larsen and D. Swann, "Applying power system stabilizers part i:general concepts," *Power Apparatus and Systems, IEEE Transactions on*, no. 6, pp. 3017–3024, 1981.

[24] E. Larsen and D. Swann, "Applying power system stabilizers part ii: Performance objectives and tuning concepts," *Power Apparatus and Systems, IEEE Transactions on*, no. 6, pp. 3025–3033, 1981.

[25] E. Larsen and D. Swann, "Applying power system stabilizers part iii: Practical considerations," *Power Apparatus and Systems, IEEE Transactions on*, no. 6, pp. 3034–3046, 1981.

[26] B. Chaudhuri and B. C. Pal, "Robust damping of multiple swing modes employing global stabilizing signals with a tcsc," *Power Systems, IEEE Transactions on*, vol. 19, no. 1, pp. 499–506, 2004.

[27] B. Chaudhuri, B. C. Pal, A. C. Zolotas, I. M. Jaimoukha, and T. C. Green, "Mixed-sensitivity approach to h control of power system oscillations employing multiple facts devices," *Power Systems, IEEE Transactions on*, vol. 18, no. 3, pp. 1149–1156, 2003.

[28] J. Deng and X.-P. Zhang, "Robust damping control of power system with tcsc using a multi-model system approach," in *AC and DC Power Transmission (ACDC 2012), 10th IET International Conference on*, pp. 1–6, IET, 2012.

[29] K. Padiyar and R. Varma, "Damping torque analysis of static var system controllers," *Power Systems, IEEE Transactions on*, vol. 6, no. 2, pp. 458–465, 1991.

[30] G. N. Taranto, J.-K. Shiau, J. H. Chow, and H. Othman, "Robust decentralised design for multiple facts damping controllers," *IEE Proceedings-Generation, Transmission and Distribution*, vol. 144, no. 1, pp. 61–67, 1997.

[31] E.-Z. Zhou, "Application of static var compensators to increase power system damping," *Power Systems, IEEE Transactions on*, vol. 8, no. 2, pp. 655–661, 1993.

[32] J. Smith, D. Pierre, D. Rudberg, I. Sadighi, A. Johnson, and J. Hauer, "An enhanced lq adaptive var unit controller for power system damping," *Power Systems, IEEE Transactions on*, vol. 4, no. 2, pp. 443–451, 1989.

[33] J. Smith, D. Pierre, I. Sadighi, and M. Nehrir, "A supplementary adaptive var unit controller for power system damping," *Power Systems, IEEE Transactions on*, vol. 4, no. 3, pp. 1017–1023, 1989.

[34] X. Yu, M. Khammash, and V. Vittal, "Robust design of a damping controller for static var compensators in power systems," *Power Systems, IEEE Transactions on*, vol. 16, no. 3, pp. 456–462, 2001.

[35] J. Sefton and K. Glover, "Pole/zero cancellations in the general h problem with reference to a two block design," *Systems & Control Letters*, vol. 14, no. 4, pp. 295–306, 1990.

[36] L. A. L. Tenorio, "Hydro turbine and governor modelling," 2010.

[37] K. Glover, "All optimal hankel-norm approximations of linear multivariable systems and their l,-error bounds," *International journal of control*, vol. 39, no. 6, pp. 1115–1193, 1984.

[38] I. Kamwa, A. Heniche, G. Trudel, M. Dobrescu, R. Grondin, and D. Lefebvre, "Assessing the technical value of facts-based wide-area damping control loops," in *Power Engineering Society General Meeting, 2005. IEEE*, pp. 1734–1743, IEEE, 2005.

[39] J. J. Sanchez-Gasca and J. H. Chow, "Power system reduction to simplify the design of damping controllers for interarea oscillations," *Power Systems, IEEE Transactions on*, vol. 11, no. 3, pp. 1342–1349, 1996.

[40] R. Y. Chiang and M. G. Safonov, *Robust Control Toolbox: for Use with MATLAB: User's Guide, June 1, 1988*. MathWorks Incorporated, 1988.

[41] T.-G. Park, "Estimation strategies for fault isolation of linear systems with disturbances," *IET control theory & applications*, vol. 4, no. 12, pp. 2781–2792, 2010.

[42] I. Kamwa, R. Grondin, and Y. Hébert, "Wide-area measurement based stabilizing control of large power systems-a decentralized/hierarchical approach," *Power Systems, IEEE Transactions on*, vol. 16, no. 1, pp. 136–153, 2001.

[43] G. Heydt, C. Liu, A. Phadke, and V. Vittal, "Solution for the crisis in electric power supply," *Computer Applications in Power, IEEE*, vol. 14, no. 3, pp. 22–30, 2001.

[44] J. H. Chow, J. J. Sanchez-Gasca, H. Ren, and S. Wang, "Power system damping controller design-using multiple input signals," *Control Systems, IEEE*, vol. 20, no. 4, pp. 82–90, 2000.

[45] Y. Zhang, *Design of wide-area damping control systems for power system low-frequency inter-area oscillations*. PhD thesis, Washington State University, 2007.

[46] N. Martins and L. T. Lima, "Determination of suitable locations for power system stabilizers and static var compensators for damping electromechanical oscillations in large scale power systems," *Power Systems, IEEE Transactions on*, vol. 5, no. 4, pp. 1455–1469, 1990.

[47] I. Kamwa, L. Gerin-Lajoie, and G. Trudel, "Multi-loop power system stabilizers using wide-area synchronous phasor measurements," in *American Control Conference, 1998. Proceedings of the 1998*, vol. 5, pp. 2963–2967, IEEE, 1998.

[48] S. Lee and C.-C. Liu, "An output feedback static var controller for the damping of generator oscillations," *Electric power systems research*, vol. 29, no. 1, pp. 9–16, 1994.

[49] M. Tarokh, "Measures for controllability, observability and fixed modes," *Automatic Control, IEEE Transactions on*, vol. 37, no. 8, pp. 1268–1273, 1992.

[50] A. Heniche and I. Karnwa, "Control loops selection to damp inter-area oscillations of electrical networks," *Power Systems, IEEE Transactions on*, vol. 17, no. 2, pp. 378–384, 2002.

[51] A. Hamdan and A. Elabdalla, "Geometric measures of modal controllability and observability of power system models," *Electric power systems research*, vol. 15, no. 2, pp. 147–155, 1988.

[52] R. Toscano, "Signal and system norms," in *Structured Controllers for Uncertain Systems*, pp. 25–44, Springer, 2013.

[53] W. Holderbaum, K. Hunt, and H. Gollee, "H robust control design for unsupported paraplegic standing: experimental evaluation," *Control Engineering Practice*, vol. 10, no. 11, pp. 1211–1222, 2002.

[54] B. Pal and B. Chaudhuri, "Mixed-sensitivity approach using linear matrix inequalities," *Robust Control in Power Systems*, pp. 115–138, 2005.

[55] Z. Gu and S. O. Oyadiji, "Active suspension of output feedback robust control based on lmi approach," in *ASME 7th Biennial Conference on Engineering Systems Design and Analysis*, pp. 861–868, American Society of Mechanical Engineers, 2004.

[56] M. Chilali and P. Gahinet, "H design with pole placement constraints: an lmi approach," *Automatic Control, IEEE Transactions on*, vol. 41, no. 3, pp. 358–367, 1996.

[57] J. Paserba *et al.*, "Analysis and control of power system oscillation," *CIGRE special publication*, vol. 38, no. 07, 1996.

[58] P. Kundur, M. Klein, G. Rogers, and M. S. Zywno, "Application of power system stabilizers for enhancement of overall system stability," *Power Systems, IEEE Transactions on*, vol. 4, no. 2, pp. 614–626, 1989.

[59] S. T. Cha, J. Østergaard, Q. Wu, and F. Mara, "A real-time simulation platform for power system operation," in *IPEC, 2010 Conference Proceedings*, pp. 909–914, IEEE, 2010.